STRAPDOWN FIXED GAIN AHRS WITH GPS HORIZONTAL VELOCITY AND MAGNETOMETER HEADING AIDING

Paul G. Savage
Strapdown Associates, Inc.

WBN-14029
www.strapdownassociates.com
September 4, 2021

ABSTRACT

This article provides a detailed description of a fixed gain Attitude/Heading Reference System (FGAHRS) using commercially available MEMS (micro-machined electro-mechanical system) inertial sensors (gyros and accelerometers) mounted within a strapdown inertial measurement unit (IMU). The FGAHRS is GPS velocity aided with reference heading provided by a strapdown 3-axis magnetometer. Differential equations are derived for FGAHRS computational operations with a corresponding error model for performance analysis and fixed gain determination. Equivalent FGAHRS digital computational algorithms are presented for implementation in the FGAHRS digital processor. Performance is extensively analyzed using a unique surface motion (at sea or on land) trajectory generator providing FGAHRS IMU inertial sensor inputs and a corresponding attitude/velocity/position time history. FGAHRS accuracy is assessed using the simulated IMU sensor inputs modified to include specified sensor/system errors. Simulation results are presented demonstrating 1 degree FGAHRS accuracy under dynamic trajectory conditions using gyros and accelerometers with 1 deg/sec and 10 milli-g accuracy.

TABLE OF CONTENTS

1. INTRODUCTION

With advancements in computer micro-processor technology (in speed and memory capacity), the strapdown equivalent of the mechanical AHRS (Attitude Heading Reference System) has come into being for compatibility with new strapdown (directly vehicle mounted) inertial sensor technologies. For a conventional strapdown AHRS, attitude (the combined equivalent of roll, pitch, and heading) are calculated in the AHRS computer using 3-axis inputs from gyros contained within a strapdown IMU (Inertial Measurement Unit). A representative conventional strapdown AHRS configuration is depicted in Fig. 1. Using Section 2 notation, Section 3 analytically describes the Fig. 1 configuration.

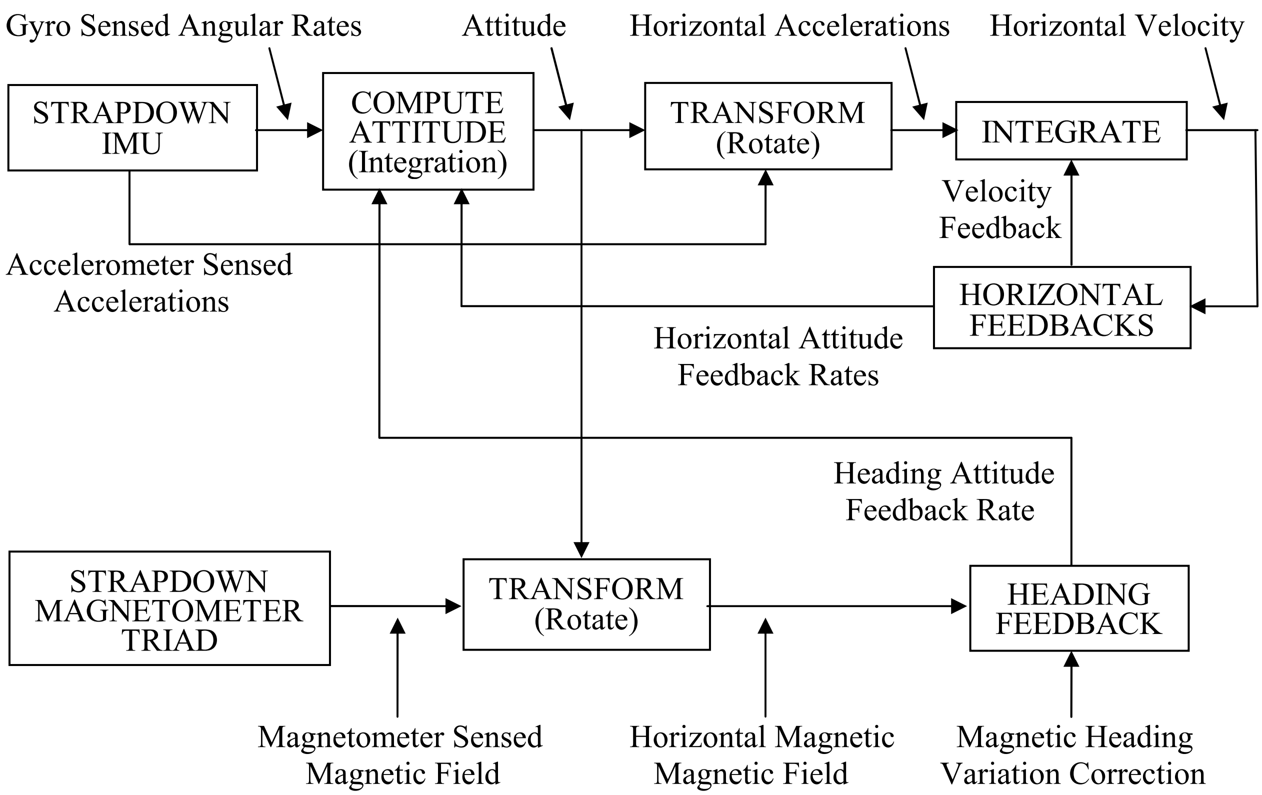

Fig. 1 – Representative Conventional Strapdown AHRS Configuration

To combat gyro bias induced roll/pitch error (horizontal attitude "tilt"), Fig. 1 applies feedback designed to maintain roll/pitch referencing to an average vertical. The horizontal tilt feedback signals are calculated using outputs from a strapdown accelerometer triad contained within the AHRS IMU. The AHRS computed attitude is used to transform (rotate) the accelerometer signals into north/east/down coordinates. The AHRS attitude tilt measurement/control concept is that for error-free attitude data, the horizontal transformed accelerations will, on the average, be zero. Thus, non-zero values measure attitude tilt for feedback correction. Low gain feedback provides the averaging mechanism to attenuate short duration horizontal acceleration deviations from the average zero. But the gains must also be large enough to combat gyro bias induced attitude tilt buildup.

To combat gyro bias induced heading error, the Fig. 1 AHRS applies feedback designed to maintain heading referencing to true north as measured with a strapdown magnetometer triad. The heading error measurement concept is that a strapdown magnetometer will measure earth's magnetic field vector whose east component differs from true east by the magnetic variation angle ("magvar" also known as magnetic declination). Thus, a mavar corrected east magnetometer measurement should ideally be zero, and a non-zero value will measure AHRS heading error for feedback correction. The east measurement is calculated using AHRS computed attitude to transform the magnetometer outputs into north/east/down coordinates. Note, however, that the transformation operation will not only generate a heading error measurement, it will also induce a north attitude tilt into the heading error measurement by projecting the vertical magnetic field component onto the east axis. The result couples attitude tilt into the heading feedback control loops, translating maneuver induced tilt into heading error. The heading error then couples back into the attitude tilt control loops. Thus, accurate tilt control is not only important to maintain good roll/pitch accuracy, it is also required for accurate strapdown magnetometer referenced heading error control.

The conventional strapdown AHRS Fig. 1 feedback concept relies on the average horizontal acceleration being small during operation. This assumption becomes increasingly invalid under sustained dynamic maneuvering. To eliminate maneuver induced errors, GPS velocity compensation can be included within the AHRS feedback structure. This article describes a GPS aided strapdown AHRS designed for operation in mobile surface vehicles (at sea or on land). As with the conventional strapdown AHRS, the GPS aided AHRS described in this article also incorporates strapdown magnetometer derived magnetic heading error measurements to combat heading error drift. The concept is depicted in Fig. 2. Section 4 analytically describes the Fig. 2 configuration.

For the most part, GPS velocity aiding has been applied in the past to strapdown AHRSs having reasonably accurate gyros/accelerometers (e.g., 10 deg/hr and 1 milli-g bias errors). The IMU investigated in this article uses commercially available MEMS (micro-machined electro-mechanical system) gyros/accelerometers having comparatively large errors (on the order of 10 deg/sec and 10 mill-g). Application of such a low accuracy IMU presents some interesting design challenges.

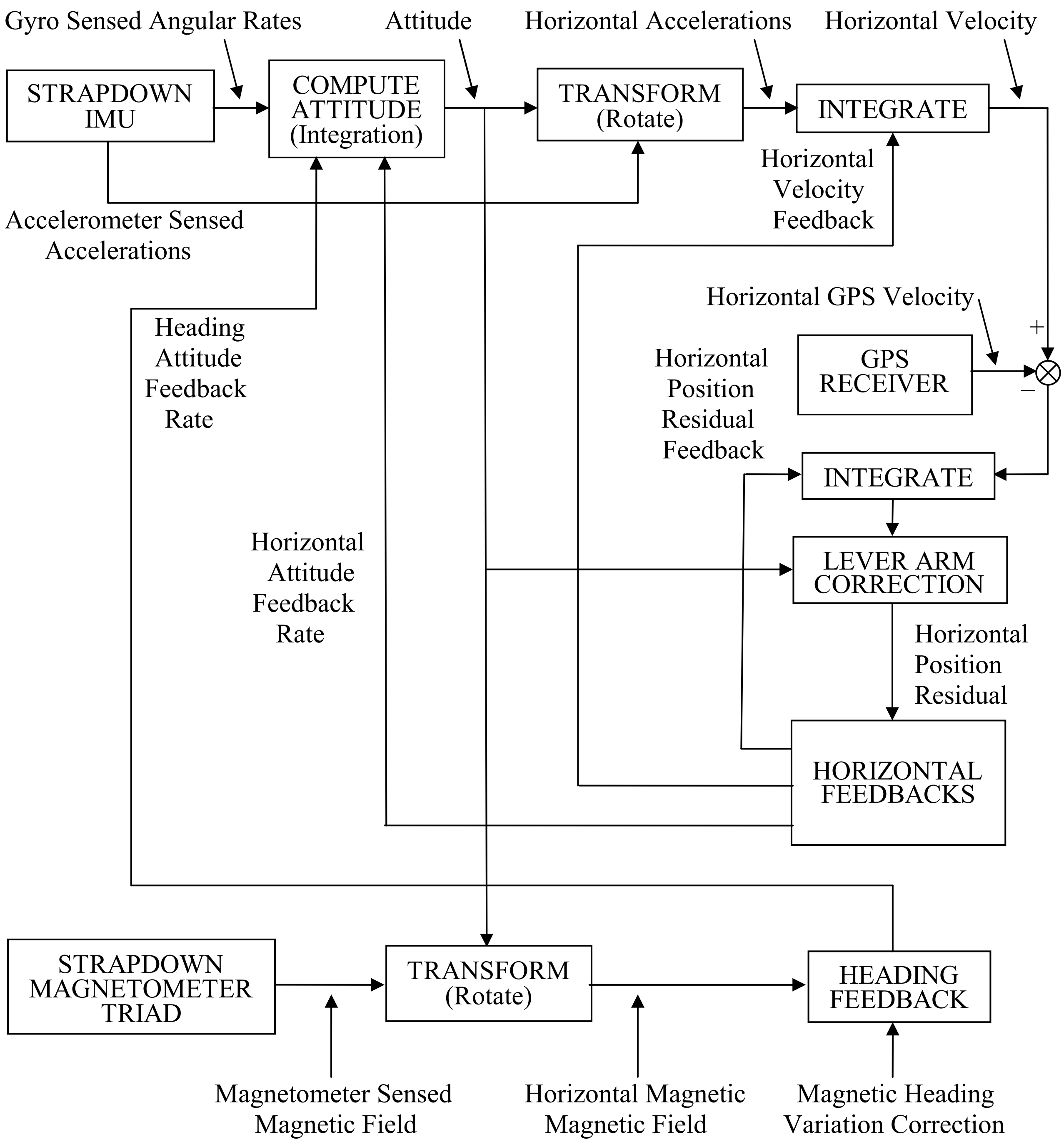

Fig. 2 – Representative GPS Aided Strapdown AHRS Configuration

The general feedback arrangement in past GPS aided strapdown AHRSs has been commonly configured within a Kalman filter structure based on known statistical properties of system/sensor error sources. Due to the uncertainty in statistical error models associated with commercially available MEMS inertial components (from different evolving manufacturers having different design configurations), it was believed that Kalman filter based AHRS feedback introduced an unnecessary degree of risk (and complexity). Hence, the GPS aided AHRS investigated in this article uses constant (fixed) gain feedback - defined as an FGAHRS (strapdown Fixed Gain AHRS) approach, the label used for the Section 4, Fig. 4 analytical flow diagram.

As for the conventional AHRS in Section 3, the GPS aided FGAHRS configuration is analytically described in Section 4 in the form of continuous integral equations. Section 5 defines an instantaneous FGAHRS coarse initialization process for the Section 4 integrators using magnetometer, IMU gyro, and GPS velocity measurements. For software implementation in the FGAHRS digital processor, Section 6 defines a digital incremental equivalent of the Section 4 continuous form analytical integral equations. Error models for the Section 4 FGAHRS are described in Section 7 (and derived in Appendices A – C). Based on the Section 7 error models, Section 8 derives equations for calculating FGAHRS closed-loop gains for specified closed-loop time response characteristics.

Even though GPS velocity feedback eliminates maneuver induced errors, FGAHRS system errors can still impact attitude accuracy, particularly when using a low-cost commercially available MEMS IMU. This is particularly true for gyro bias that can have significant day-to-day variations and in-use performance trending (e.g., from temperature changes). The problem is mitigated for the FGAHRS configuration addressed in this article, using an in-use automatic gyro calibration process described in Section 9.

Large unstable MEMS accelerometer bias errors can also significantly impact FGAHRS attitude accuracy, particularly under high/low latitudes where earth's magnetic field vector has a large vertical component. Then attitude tilt generated from accelerometer bias will couple into magnetometer measured heading control loop feedback, producing heading error that, under horizontal accelerations, couples back into the attitude tilt control loops. Section 10 discusses the problem in more detail, leading to an in-use automatic accelerometer bias compensation technique for solution (for implementation within FGAHRS software). The compensation approach is based on horizontal feedback least squares error averaging over selected time intervals as will be described in a subsequent article. That article will also show how least squares averaging can be applied during FGAHRS-vehicle-installation to automatically calibrate magnetometer detected stray magnetic field bias (plus the equivalent magnetometer-to-IMU heading misalignment). For GPS antennas mounted remotely from the IMU, the future article will also show how least squares averaging can be used to measure/calibrate the GPS-antenna-to-IMU "lever arm" displacement (GPS velocity measurement correction).

Section 11 provides an extensive numerical assessment of FGAHRS attitude accuracy along a 3 minute simulated dynamic trajectory composed of a sequence of horizontal turns coupled with 3-axis angular and linear oscillations. (A subsequent article will analytically describe the trajectory generator simulation program used to create the trajectory used for performance analysis.)

In Section 11, FGAHRS performance along the trajectory is presented in three parts. The first assesses the general effectiveness of AHRS GPS velocity aiding by comparing Fig. 4 GPS aided FGAHRS attitude accuracy with that of the Fig. 3 conventional AHRS (without GPS aiding), both operating under "nominal" error free component conditions for zero earth magnetic field inclination angle.

The second part of Section 11 expands on the "nominal" FGAHRS configuration, adding "baseline" component errors representative of low-cost commercially available MEMS IMUs, GPS-antenna-to-IMU lever arm uncertainty, and magnetometer-to-IMU heading misalignment (or the equivalent of stray magnetic field bias). To mitigate the effect of the largest FGAHRS component error sources, the second part assumes application of automatic in-use gyro/accelerometer bias compensation, and automatic GPS lever arm and magnetometer misalignment calibration during FGAHRS/user-vehicle installation.

Part three of Section 11 assesses FGAHRS performance under variations from the baseline for operation with 1 deg/sec gyro bias, 10 milli-g accelerometer bias, 10 ft GPS antenna-to-IMU lever arm uncertainty, and 5 deg magnetometer heading misalignment, all without automatic gyro/accelerometer bias compensation. Included is a baseline configuration performance assessment for zero and 74.71 deg magnetic field inclination angles (versus 58.94 deg used for baseline performance evaluation), and for larger trajectory oscillations.

Section 12 provides conclusions for the article.

2. NOTATION, COORDINATE FRAMES, AND PARAMETER DEFINITIONS

This section defines the notation and coordinate frames used throughout the article. Parameter definitions are provided in the article where they are derived.

2.1 NOTATION

$\underline{V} =$ Vector having length and direction.

$\underline{V}^A =$ Column matrix with elements equal to projections of $\underline{V}$ on coordinate frame A axes, i.e., the dot product of $\underline{V}$ with a unit vector parallel to each coordinate axis.

$\left(\underline{V}^A \times\right) =$ Skew symmetric (or cross-product) square matrix form of $\underline{V}^A$ represented by $\begin{bmatrix} 0 & -V_{ZA} & V_{YA} \\ V_{ZA} & 0 & -V_{XA} \\ -V_{YA} & V_{XA} & 0 \end{bmatrix}$ where $-V_{XA}$, V_{YA}, V_{ZA} are components of $\underline{V}^A$. The matrix product of $\left(\underline{V}^A \times\right)$ with another A frame projected vector equals the cross-product of $\underline{V}^A$ with the vector, i.e., $\left(\underline{V}^A \times\right) \underline{W}^A = \underline{V}^A \times \underline{W}^A$.

$C_{A2}^{A1} =$ Frame A_2 to A_1 direction cosine matrix (DCM) that transforms a vector from its A_2 projection to its A_1 projection, i.e., $\underline{V}^{A1} = C_{A2}^{A1}\, \underline{V}^{A2}$. An important property of C_{A2}^{A1} is that its inverse equals its transpose.

$\dot{(\,)}$ = Derivative $\frac{d(\,)}{dt}$ of parameter ( ) with respect to time t.

H = Subscript denoting a vector or matrix in which the vertical component or row is equated to zero.

k = IMU inertial sensor output cycle index (e.g., 1000 KHz k cycle rate). Used as a subscript, it indicates the value of a sensor output sample at the end of a k cycle.

m = AHRS algorithm update cycle index (e.g., 100 Hz m cycle rate). Used as a subscript, it indicates the value of a parameter at the end of an m update cycle.

t = Time from start of the FGAHRS algorithms computations.

2.2 COORDINATE FRAMES

B = Sensor frame fixed relative to IMU inertial sensor axes, rotating with the IMU. The B frame angular orientation relative to sensor axes is arbitrary based on user preferences.

N = Earth fixed coordinate frame with axes aligned with local north(x), east(y), down(z) directions.

3. CONVENTIONAL STRAPDOWN AHRS ANALYTICAL STRUCTURE

The conventional AHRS configuration (used in this article for FGAHRS comparison) is built around an inertial calculation of attitude/velocity using orthogonal three-axis gyros/accelerometer inputs from a strapdown IMU. Gravity is approximated as being vertical; the effect of earth's rotation and vehicle angular translation over earth's surface (order of 10 deg/hr) is ignored compared to the accuracy capability of commercially available MEMS gyros considered in this article. Based on these approximations, the AHRS analytical structure simplifies to the configuration depicted in Fig. 3.

In Fig. 3, C_B^N is a direction cosine matrix that transforms vectors from strapdown IMU B frame coordinates to locally level non-rotating N frame axes, $\underline{a}_{Accel}^B$ is the IMU accelerometer output vector in B frame coordinates (sensing non-gravitational acceleration – "specific force"), $\underline{a}_{Accel}^N$ is the IMU sensed specific force transformed to the N frame, $\left(\underline{a}_{Accel}^N\right)_H$ is the horizontal component of $\underline{a}_{Accel}^N$ (also, the total horizontal acceleration as there is no horizontal gravity component), $\underline{v}_H^N$ is horizontal velocity (the integral of horizontal acceleration $\dot{\underline{v}}_H^N$) in the N frame, and subscript 0 indicates the initial value of the designated parameter at time $t = 0$.

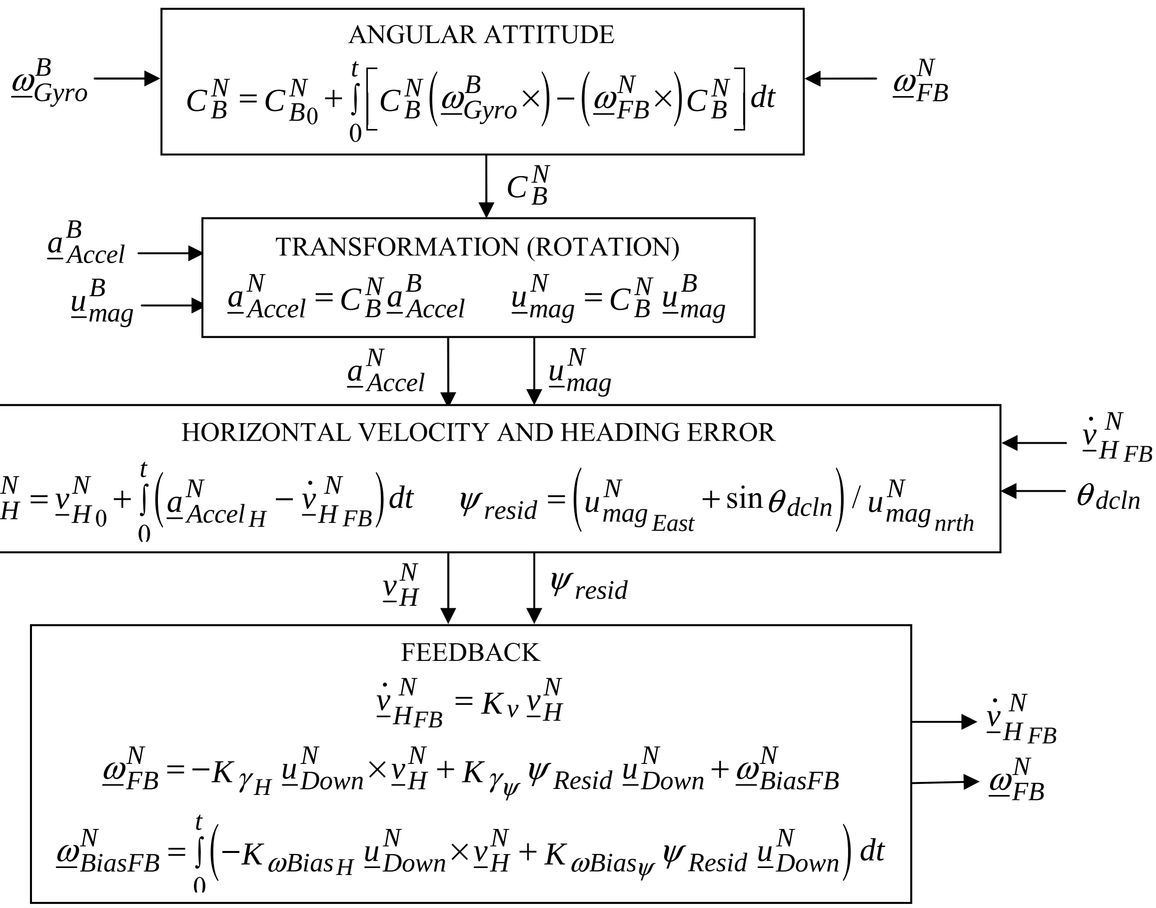

Fig. 3 – Representative Conventional Strapdown AHRS

The C^N_B matrix in Fig. 3 is updated for IMU measured strapdown inertial rotation rate $\underline{\omega}^B_{Gyro}$ using the classic direction cosine matrix angular rate formula [1, Eq. (3.3.2-9)]. The C^N_B updating process includes angular rate feedback correction vector $\underline{\omega}^N_{FB}$ whose N frame form in Fig. 3 derives as follows:

$$
\begin{aligned}
\dot{C}^N_B &= C^N_B \left[\left(\underline{\omega}^B_{Gyro} - \underline{\omega}^B_{FB} \right) \times \right] = C^N_B \left(\underline{\omega}^B_{Gyro} \times \right) - C^N_B \left(\underline{\omega}^B_{FB} \times \right) \\
&= C^N_B \left(\underline{\omega}^B_{Gyro} \times \right) - C^N_B \left(\underline{\omega}^B_{FB} \times \right) \left(C^N_B \right)^T C^N_B \\
&= C^N_B \left(\underline{\omega}^B_{Gyro} \times \right) - \left[\left(C^N_B \, \underline{\omega}^B_{FB} \right) \times \right] C^N_B \\
&= C^N_B \left(\underline{\omega}^B_{Gyro} \times \right) - \left(\underline{\omega}^N_{FB} \times \right) C^N_B
\end{aligned} \tag{1}
$$

Basic $\underline{\omega}_{Gyro}^{B}$ inertial rotation rate updating of C_B^N is first analytically shown in (1) as being augmented in the *B* frame by angular rate feedback correction $\underline{\omega}_{FB}^{B}$. The subsequent (1) derivation then employs well-known mathematical corollaries that the inverse of a direction cosine matrix equals its transpose [1, Eq. (3.1-15)], and that $C_B^N \left(\underline{\omega}_{FB}^{B} \times \right) \left(C_B^N \right)^T$ (the matrix transpose of the cross-product form of $\underline{\omega}_{FB}^{B}$) equals the cross-product form of $C_B^N \, \underline{\omega}_{FB}^{B}$ [1, Eq. (3.1.1-40)]. The final derived (1) result is what is represented in Fig. 3.

The computed C_B^N matrix in Fig. 3 is used to transform the IMU accelerometer measurements $\underline{a}_{Accel}^{B}$ and the vector outputs from the strapdown magnetometer triad $\underline{u}_{mag}^{B}$ into *N* frame (north, east, down) components $\underline{a}_{Accel}^{N}$ and $\underline{u}_{mag}^{N}$. (Note: In practice, the magnetometer triad may not be aligned with the *B* frame as are the accelerometers, hence, a fixed transformation may be required to generate $\underline{u}_{mag}^{B}$ - i.e., $\underline{u}_{mag}^{B} = C_M^B \, \underline{u}_{mag}^{M}$ where *M* is a coordinate frame aligned with magnetometer triad input axes.) The $\underline{a}_{Accel}^{N}$ result in Fig. 3 is integrated to generate horizontal velocity components $\underline{v}_H^N$, and $\underline{u}_{mag}^{N}$ is used to calculate the ψ_{resid} heading error in the AHRS computed C_B^N matrix (after providing correction for earth's magnetic field vector $\underline{u}_{mag}^{N}$ declination θ_{dcln} from true north). (The $u_{mag_{nrth}}^{N}$ parameter in the ψ_{resid} calculation is a unit vector along the *N* frame north (x) axis.) The $\underline{v}_H^N$ integration process in Fig. 3 includes feedback correction $\dot{\underline{v}}_{H_{FB}}^{N}$ to maintain average C_B^N vertical referencing to the local horizontal.

The computed $\underline{v}_H^N$ and ψ_{resid} signals are then used through fixed gains K_v, K_{γ_H}, K_{γ_ψ}, $K_{\omega Bias_H}$, $K_{\omega Bias_\psi}$ to generate the $\underline{\omega}_{FB}^{N}$ and $\dot{\underline{v}}_{H_{FB}}^{N}$ feedbacks in Fig. 3. Basing the feedback on integrated acceleration $\underline{v}_H^N$ (rather than on $\underline{a}_{Accel_H}^{N}$ directly), attenuates transitory $\underline{a}_{Accel_H}^{N}$ components from impacting C_B^N accuracy. The $\underline{u}_{Down}^{N}$ parameter in Fig. 3 represents a unit vector along the *N* frame downward axis z. Its cross-product operator presence when computing $\underline{\omega}_{FB}^{N}$ feedback, rotates the $\underline{v}_H^N$ multiplicand around the vertical by 90 degrees, the required analytical orientation for translating linear $\underline{v}_H^N$ feedback into a corresponding *N* frame angular rotation.

Note that Fig. 3 includes an integration operation for estimating *N* frame components of the IMU strapdown gyro bias vector $\underline{\omega}_{BiasFB}^{N}$. Including this term within the $\underline{\omega}_{FB}^{N}$ feedback prevents actual gyro bias from inducing attitude "hang-off" error in the closed-loop feedback operations. The $\underline{\omega}_{BiasFB}^{N}$ signal will form the basis for the in-use automatic gyro compensation routine discussed in Section 9.

Roll, pitch, heading (ϕ, θ, ψ) AHRS outputs (not shown in Fig. 3) would derive from the C_B^N equivalency in [1, Eq. (3.2.3.1-2)]:

$$C_B^N = \begin{bmatrix} \cos\theta\cos\psi & -\cos\phi\sin\psi + \sin\phi\sin\theta\cos\psi & \sin\phi\sin\psi + \cos\phi\sin\theta\cos\psi \\ \cos\theta\sin\psi & \cos\phi\cos\psi + \sin\phi\sin\theta\sin\psi & -\sin\phi\cos\psi + \cos\phi\sin\theta\sin\psi \\ -\sin\theta & \sin\phi\cos\theta & \cos\phi\cos\theta \end{bmatrix} \quad (2)$$

From (2),

$$\begin{aligned} &\phi = \sin^{-1}\frac{C_{32}}{\sqrt{C_{11}^2 + C_{21}^2}} \qquad \theta = -\sin^{-1} C_{31} \quad \text{Using 2 Quadrant ArcSin Extraction} \\ &\psi = \tan^{-1}\frac{C_{21}}{C_{11}} \quad \text{Using 4 Quadrant ArcTan Extraction} \end{aligned} \quad (3)$$

where C_{11}, C_{21}, C_{32} are elements in column 1, rows 1 and 2, and in column 2, row 3 of the C_B^N matrix.

4. GPS VELOCITY AIDED STRAPDOWN FGAHRS ANALYTICAL STRUCTURE

In contrast with the conventional AHRS in Fig. 3, the strapdown FGAHRS configuration incorporates GPS horizontal velocity in the feedback structure to mitigate horizontal acceleration induced attitude error. The basic FGAHRS concept is depicted analytically in Fig. 4. FGAHRS roll, pitch, heading outputs from Fig. 4 would derive from the same Eqs. (3) provided for the Fig. 3 conventional strapdown AHRS.

In Fig. 4, the basic FGAHRS vertical attitude control feedback signal is a horizontal position "like" parameter $\underline{R}_{Resid_H}^{N}$ ("position change residual") generated from $\Delta\underline{R}_{woLv_H}^{N}$, the integral of $\underline{v}_H^N$ corrected for measured GPS horizontal velocity $\underline{v}_{GPS_H}^{N}$ and $\Delta\dot{\underline{R}}_{woLv/H_{FB}}^{N}$ feedback. (The *woLv* subscript refers to the integral <u>without lever-arm</u> correction for the distance vector from the GPS antenna to the IMU.) The $\underline{R}_{Resid_H}^{N}$ signal only measures the effect of propagated FGAHRS component errors (in the IMU, GPS velocity, strapdown magnetometer triad $\underline{u}_{mag}^{B}$ measurements), with <u>no direct response to actual horizontal acceleration</u>. It is calculated by correcting $\Delta\underline{R}_{woLv_H}^{N}$ for the N frame change in $\underline{l}^B$ distance (produced by the change in C_B^N attitude since time $t = 0$). The corrected $\underline{R}_{Resid_H}^{N}$ result then becomes the source for C_B^N

horizontal attitude tilt error feedback generation. The comparable feedback signal for the conventional AHRS in Fig. 3 is $\underline{v}_H^N$. The Fig. 4 FGAHRS also generates a magnetic heading derived error signal ψ_{resid} for C_B^N heading attitude error feedback, the computation being identical to that in Fig. 3 for the conventional AHRS.

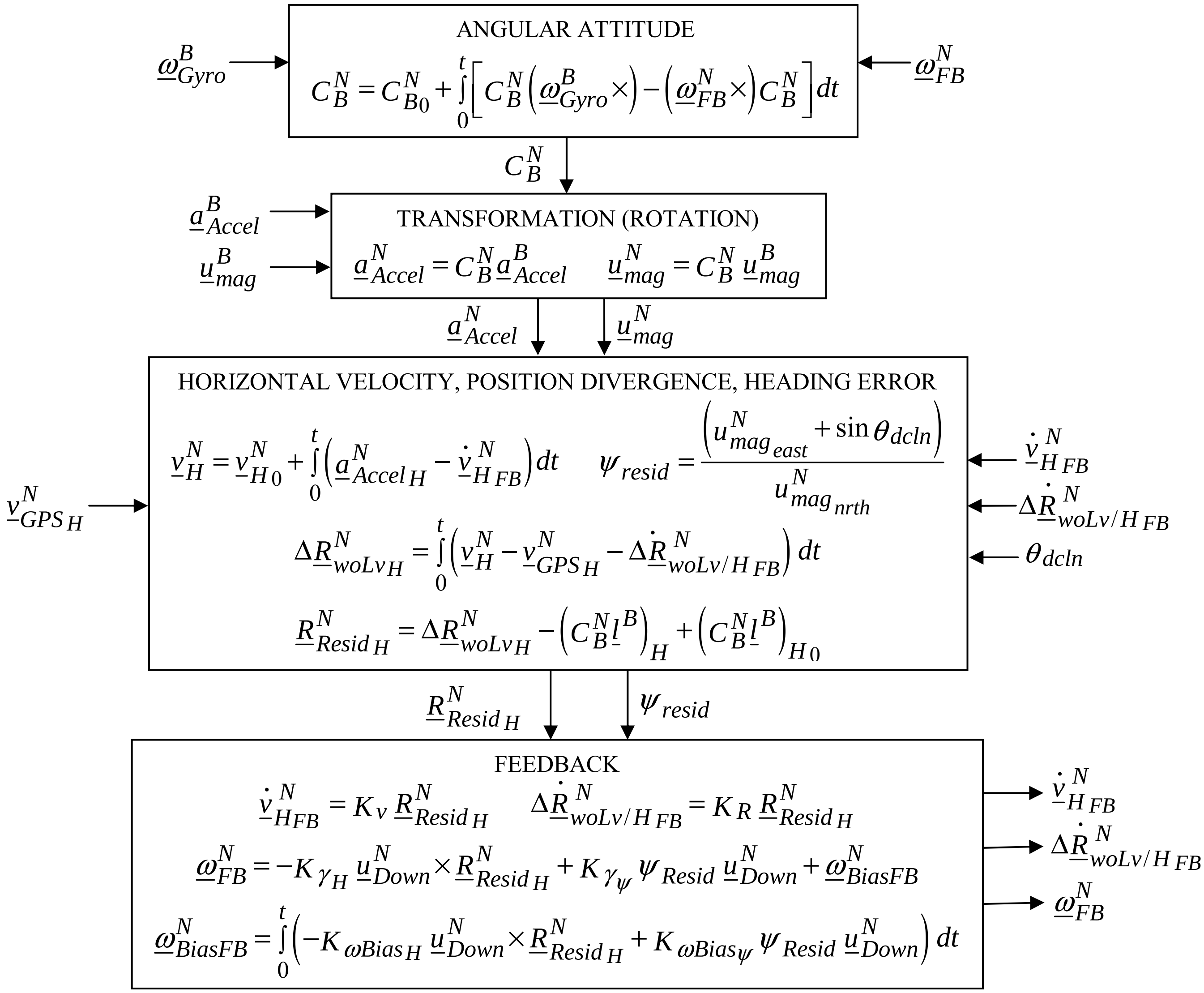

Fig. 4 – GPS Velocity Aided Strapdown FGAHRS

Computation of $\dot{\underline{v}}_{H\,FB}^N$, $\underline{\omega}_{FB}^N$ feedbacks in Fig. 4 matches the conventional AHRS equivalent in Fig. 3, the exception being that the K_v, K_{γ_H} gains now multiply $\underline{R}_{Resid\,H}^N$ rather than $\underline{v}_H^N$, and an added feedback gain K_R is applied for generating $\Delta \dot{\underline{R}}_{woLv/H\,FB}^N$. For compatibility with the added K_R feedback and associated fourth order (4 feedbacks) dynamic feedback response, the Fig. 4 K_v, K_{γ_H}, $K_{\omega Bias_H}$ gain values would differ from those in Fig. 3 (designed for a 3 feedback third order dynamic response characteristic).

An alternative to the Fig. 4 configuration that more closely mimics the Fig. 3 approach would be to structure the horizontal attitude tilt correction loop using GPS corrected horizontal velocity feedback, i.e., in place of the integrated velocity feedback arrangement in Fig. 4. As in Fig. 4, that GPS correction would also account for lever-arm motion, however, now representing lever arm velocity rather than position change. Lever arm velocity would compute as the cross-product of gyro-measured angular rate with the lever arm distance vector. However, under un-modelable high frequency lever arm bending, the computed lever-arm velocity correction would produce high frequency bending feedback noise error, a disadvantage for the velocity feedback approach. The same error would also appear in the Fig. 4 integrated velocity feedback approach, however, at a much attenuated amplitude. An additional advantage afforded by the Fig. 4 integrated velocity feedback approach is that the lever-arm compensation error will appear directly in the $\underline{R}^N_{Resid_H}$ measurement. This allows the lever-arms to be easily in-use calibrated using least squares error averaging as part of FGAHRS installation procedures (to be described in the forthcoming article on in-use automatic FGAHRS accelerometer calibration).

5. FGAHRS INITIALIZATION

Before the Fig. 4 FGAHRS integration process begins, the C^N_B, $\underline{v}^N_H$ initial values (C^N_{B0}, $\underline{v}^N_{H0}$) must be set. Setting C^N_{B0} is performed using a Coarse Attitude Initialization process based on magnetometer detected outputs. The $\underline{v}^N_{H0}$ value is set using the computed coarse C^N_{B0} value, measured GPS velocity, and IMU measured angular rates (for GPS receiver-to-IMU lever arm correction). Details are described next.

5.1 COARSE ATTITUDE INITIALIZATION

Coarse Attitude Initialization approximates the initial roll/pitch angles in C^N_{B0} as zero. Based on the form of (2), for zero roll, pitch we can write:

$$\hat{C}^N_{B0} = \begin{bmatrix} \cos\hat{\psi}_0 & -\sin\hat{\psi}_0 & 0 \\ \sin\hat{\psi}_0 & \cos\hat{\psi}_0 & 0 \\ 0 & 0 & 1 \end{bmatrix} \tag{4}$$

where $\hat{C}^N_{B0}$ is the coarse aligned value for C^N_{B0}, and $\hat{\psi}_0$ is the corresponding coarse initial heading. Using $\hat{C}^N_{B0}$ to transform strapdown magnetometer triad output $\underline{u}^B_{mag}$ into the *N* frame gives

$$\hat{u}_{mag}^{N} = \hat{C}_{B0}^{N}\, \underline{u}_{mag}^{B} \tag{5}$$

where $\hat{u}_{mag}^{N}$ is an approximation to the actual transformed $\underline{u}_{mag}^{N}$ value. But at time $t = 0$, $\underline{u}_{mag}^{B} = \left(C_{B0}^{N}\right)^{T} \underline{u}_{mag}^{N}$ (i.e., based on the true C_{B0}^{N} and $\underline{u}_{mag}^{N}$ values at that time). Substituting $\hat{C}_{B0}^{N}$ from (4) and $\underline{u}_{mag}^{N}$ from (C-2) of Appendix C into (5) obtains

$$\begin{aligned}
\hat{\underline{u}}_{mag}^{N} = \hat{C}_{B0}^{N}\, \underline{u}_{mag}^{B} &= \begin{bmatrix} \cos\hat{\psi}_0 & -\sin\hat{\psi}_0 & 0 \\ \sin\hat{\psi}_0 & \cos\hat{\psi}_0 & 0 \\ 0 & 0 & 1 \end{bmatrix} \begin{bmatrix} \cos\theta_{dcln}\cos\theta_{incln} \\ -\sin\theta_{dcln} \\ \cos\theta_{dcln}\sin\theta_{incln} \end{bmatrix} \\
&= \begin{bmatrix} \cos\theta_{dcln}\cos\theta_{incln}\cos\hat{\psi}_0 + \sin\theta_{dcln}\sin\hat{\psi}_0 \\ \cos\theta_{dcln}\cos\theta_{incln}\sin\hat{\psi}_0 - \sin\theta_{dcln}\cos\hat{\psi}_0 \\ \cos\theta_{dcln}\sin\theta_{incln} \end{bmatrix}
\end{aligned} \tag{6}$$

The first two (x, y) components of $\hat{u}_{mag}^{N}$ are from (6):

$$\begin{aligned}
\hat{u}_{mag_x}^{N} &= \cos\theta_{dcln}\cos\theta_{incln}\cos\hat{\psi}_0 + \sin\theta_{dcln}\sin\hat{\psi}_0 \\
\hat{u}_{mag_y}^{N} &= \cos\theta_{dcln}\cos\theta_{incln}\sin\hat{\psi}_0 - \sin\theta_{dcln}\cos\hat{\psi}_0
\end{aligned} \tag{7}$$

Using Cramer's rule (or a step-by-step analytical equivalent), Eqs. (7) can be easily solved for $\sin\hat{\psi}_0$ and $\cos\hat{\psi}_0$:

$$\begin{aligned}
\sin\hat{\psi}_0 &= \frac{\hat{u}_{mag_x}^{N}\sin\theta_{dcln} + \hat{u}_{mag_y}^{N}\cos\theta_{dcln}\cos\theta_{incln}}{\left(\cos^2\theta_{dcln}\cos^2\theta_{incln} + \sin^2\theta_{dcln}\right)} \\
\cos\hat{\psi}_0 &= \frac{\hat{u}_{mag_x}^{N}\cos\theta_{dcln}\cos\theta_{incl} - \hat{u}_{mag_y}^{N}\sin\theta_{dcln}}{\left(\cos^2\theta_{dcln}\cos^2\theta_{incl} + \sin^2\theta_{dcln}\right)}
\end{aligned} \tag{8}$$

With $\sin\hat{\psi}_0$ and $\cos\hat{\psi}_0$ determined in (8), $\hat{C}_{B0}^{N}$ is calculated with (4). Coarse initial attitude alignment would then be executed using the computed $\hat{C}_{B0}^{N}$ approximation for C_{B0}^{N} in Fig. 4.

5.2 COARSE HORIZONTAL VELOCITY INITIALIZATION

Initializing FGAHRS horizontal velocity $\underline{v}_H^N$ in Fig. 4, equates $\underline{v}_{H0}^N$ to GPS receiver provided horizontal velocity $\underline{v}_{GPS_H}^N$ minus the horizontal velocity of the GPS antenna relative to the FGAHRS IMU:

$$\underline{v}_{H0}^N = \underline{v}_{GPS_H}^N - \dot{\underline{l}}_H^N \tag{9}$$

For $\underline{l}^B$ defined as the *B* frame lever arm distance vector from the GPS antenna to the IMU (considered constant in the *B* frame), $\underline{l}_H^N$ is the $\underline{l}^B$ horizontal (*H*) projection on the *N* frame, and $\dot{\underline{l}}_H^N$ is the $\underline{l}_H^N$ rate of change in (9). Since $\underline{l}^B$ is approximately constant in the *B* frame (i.e., neglecting bending effects), applying $\dot{C}_B^N$ from [1, Eq. (3.3.2-6)] to (9) gives

$$\dot{\underline{l}}_H^N = \frac{d}{dt}\left(C_B^N\,\underline{l}^B\right)_H = \left(\dot{C}_B^N\;\underline{l}^B\right)_H = \left[C_B^N\left(\underline{\omega}_{Gyro}^B\times\right)\underline{l}^B\right]_H = \left[C_B^N\left(\underline{\omega}_{Gyro}^B\times\underline{l}^B\right)\right]_H \tag{10}$$

Approximating C_B^N in (10) by $\hat{C}_{B0}^N$ from (4) with (8), and approximating $\underline{\omega}_{Gyro}^B$ in (10) by $\underline{\sigma}_m / T_m$ (the IMU integrated gyro increment output $\underline{\sigma}_m$ over the current *m* cycle divided by the *m* cycle time interval T_m), coarse velocity initialization approximates $\underline{v}_{H0}^N$ by the estimate $\hat{\underline{v}}_{H0}^N$:

$$\hat{\underline{v}}_{H0}^N = \underline{v}_{GPS_H}^N - \left[\hat{C}_{B0}^N\left(\underline{\sigma}_m\times\underline{l}^B\right)\right]_H / T_m \tag{11}$$

Coarse horizontal velocity initialization is achieved using the $\hat{\underline{v}}_{H0}^N$ approximation in (11) for $\underline{v}_{H0}^N$ in Fig. 4.

6. FGAHRS COMPUTER ALGORITHM DEFINITION

For FGAHRS software implementation, Figs. 5a and 5b provide a sequential set of digital incremental computations, the equivalent of the Fig. 4 continuous form integral equations. Fig. 5a describes FGAHRS attitude, velocity, position residual updates for IMU, magnetometer, and GPS inputs over an *m* computation cycle time interval. Fig. 5b generates and applies feedback corrections to the Fig. 5a results, completing the *m* cycle. With some notable exceptions, the analytical notation and computational flow in Figs. 5a and 5b parallels that in Fig. 4.

$\underline{\omega}_{Gyro_k} \quad \underline{a}_{Accel_k}$

$$\underline{\sigma}_m = \sum_m \frac{1}{2}\left(\underline{\omega}_{Gyro_k} + \underline{\omega}_{Gyro_{k-1}}\right) T_k$$

$$\underline{\upsilon}_k = \underline{\upsilon}_{k-1} + \frac{1}{2}\left(\underline{a}_{Accel_k} + \underline{a}_{Accel_{k-1}}\right) T_k \qquad \text{At } m \text{ cycle end: } \underline{\eta}_m = \underline{\upsilon}_k \quad \underline{\upsilon}_k = 0$$

$$\Delta\underline{\kappa}_k = \left[\underline{\upsilon}_{k-1} + \frac{1}{12}\left(5\,\Delta\underline{\upsilon}_k + \Delta\underline{\upsilon}_{k-1}\right)\right] T_k \qquad \underline{\kappa}_m = \sum_m \Delta\underline{\kappa}_k$$

$$\text{Do for } n = 1, 2, 3, 4: \quad f_n(\chi) = \frac{1}{n!} - \frac{\chi^2}{(n+2)!} + \frac{\chi^4}{(n+4)!} + \cdots$$

$$C_{B_m}^{B_{m-1}} = I + f_1(\sigma_m)\left(\underline{\sigma}_m \times\right) + f_2(\sigma_m)\left(\underline{\sigma}_m \times\right)^2$$

$$\Delta\underline{v}_{SF_m}^{B} = \left[I + f_2(\sigma_m)\left(\underline{\sigma}_m \times\right) + f_3(\sigma_m)\left(\underline{\sigma}_m \times\right)^2\right]\underline{\eta}_m$$

$$\Delta\underline{R}_{SF_m}^{B} = \left[I + 2\,f_2(\sigma_m)\left(\underline{\sigma}_m \times\right) + 2\,f_3(\sigma_m)\left(\underline{\sigma}_m \times\right)^2\right]\underline{\kappa}_m$$

$$C*_{B_m}^{N} = C_{B_{m-1}}^{N}\, C_{B_m}^{B_{m-1}}$$

$\underline{u}_{mag_m}^{B} \quad \underline{v}_{GPS/H_m}^{N}$

$$\Delta\underline{v}_{SF/H_m}^{N} = I_H\, C_{B_{m-1}}^{N}\, \Delta\underline{v}_{SF_m}^{B} \qquad \Delta\underline{R}_{SF/H_m}^{N} = I_H\, C_{B_{m-1}}^{N}\, \Delta\underline{R}_{SF_m}^{B} \qquad \underline{u}_{mag_m}^{N} = C*_{B_m}^{N}\, \underline{u}_{mag_m}^{B}$$

$$\underline{v}*_{H_m}^{N} = \underline{v}_{H_{m-1}}^{N} + \Delta\underline{v}_{SF/H_m}^{N}$$

$$\Delta\underline{R}*_{woLv/H_m}^{N} = \Delta\underline{R}_{woLv/H_{m-1}}^{N} + \Delta\underline{R}_{SF/H_m}^{N} + \underline{v}_{H_{m-1}}^{N}\, T_m - \frac{1}{2}\left(\underline{v}_{GPS/H_m}^{N} + \underline{v}_{GPS/H_{m-1}}^{N}\right)$$

$$\Delta\underline{R}*_{Resid/H_m}^{N} = \Delta\underline{R}*_{woLv/H_m}^{N} - I_H\left(C*_{B_m}^{N} - C_{B_0}^{N}\right)\underline{l}^{B} \qquad \psi_{resid_m} = \frac{\left(u_{mag/east_m}^{N} + \sin\theta_{dcln}\right)}{u_{mag/nrth_m}^{N}}$$

$C*_{B_m}^{N} \quad \underline{v}*_{H_m}^{N} \quad \underline{R}*_{woLv/H_m}^{N} \quad \Delta\underline{R}*_{Resid/H_m}^{N} \quad \psi_{resid_m}$

Fig. 5a – FGAHRS Incremental Algorithm Updating For IMU, Magnetometer, GPS Inputs

$$C^{*N}_{B_m} \quad \underline{v}^{*N}_{H_m} \quad \underline{R}^{*N}_{woLv/H_m} \quad \Delta\underline{R}^{*N}_{Resid/H_m} \quad \psi_{resid_m}$$

$$\downarrow$$

$$\underline{\omega}^N_{BiasFB_m} = \underline{\omega}^N_{BiasFB_{m-1}} + \left(-K_{\omega Bias_H} \; \underline{u}^N_{Down} \times \Delta\underline{R}^{*N}_{Resid/H_m} + K_{\omega Bias_\psi} \psi_{Resid_m} \underline{u}^N_{Down} \right) T_m$$

$$\underline{\omega}^N_{FB_m} = -K_{\gamma_H} \underline{u}^N_{Down} \times \Delta\underline{R}^{*N}_{Resid/H_m} + K_{\gamma_\psi} \psi_{Resid_m} \underline{u}^N_{Down} + \underline{\omega}^N_{BiasFB_m}$$

$$\downarrow$$

$$\underline{\beta}^N_{FB_m} = 0.5\left(\underline{\omega}^N_{FB_m} + \underline{\omega}^N_{FB_{m-1}} \right) T_m$$

$$\Delta\underline{v}^N_{H/FB_m} = 0.5 \, K_v \left(\Delta\underline{R}^{*N}_{Resid/H_m} + \Delta\underline{R}^{*N}_{Resid/H_{m-1}} \right) T_m$$

$$\Delta\underline{R}^N_{woLvFB/H_m} = 0.5 \, K_R \left(\Delta\underline{R}^{*N}_{Resid/H_m} + \Delta\underline{R}^{*N}_{Resid/H_{m-1}} \right) T_m$$

$$\downarrow$$

$$C^N_{B_m} = \left[I - f_1\left(\beta^N_{FB_m}\right)\left(\underline{\beta}^N_{FB_m} \times\right) + f_2\left(\beta^N_{FB_m}\right)\left(\underline{\beta}^N_{FB_m} \times\right)^2 \right] C^{*N}_{B_m}$$

$$E_{SYM} = \frac{1}{2}\left[C^N_{B_m} \left(C^N_{B_m} \right)^T - I \right] \qquad C^N_{B_m} = \left(I - E_{SYM} \right) C^N_{B_m}$$

$$\downarrow$$

$$\underline{v}^N_{H_m} = \underline{v}^{*N}_{H_m} - \Delta\underline{v}^N_{H/FB_m}$$

$$\underline{R}^N_{woLv/H_m} = \underline{R}^{*N}_{woLv/H_m} - \Delta\underline{R}^N_{woLvFB/H_m}$$

$$\downarrow$$

$$\phi = \sin^{-1} \frac{C_{32}}{\sqrt{C_{11}^2 + C_{21}^2}} \qquad \theta = -\sin^{-1} C_{31} \qquad \text{Using 2 Quadrant ArcSin Extraction}$$

$$\psi = \tan^{-1} \frac{C_{21}}{C_{11}} \quad \text{Using 4 Quadrant ArcTan Extraction}$$

$$\downarrow$$

$$C^N_{B_m} \quad \underline{v}^N_{H_m} \quad \underline{R}^N_{woLv/H_m} \quad \phi \quad \theta \quad \psi$$

Fig. 5b – FGAHRS Updating For Feedback And Attitude Output Generation

Referring first to Fig. 5a, the first computation block applies trapezoidal integration to convert FGAHRS IMU gyro/accelerometer inputs $\underline{\omega}_{Gyro_k}$, $\underline{a}_{Accel_k}$ taken at a k cyclic input rate (e.g., 1 khz for a 0.001 sec sample time interval T_k), into equivalent integrated angular-rate/acceleration increments over the lower frequency *m* cycle used for remaining computations (e.g., 100 hz for a 0.01 sec update cycle time interval T_m). The $\underline{\omega}_{Gyro_k}$, $\underline{a}_{Accel_k}$ integration increments are equated to rotation/velocity-translation vectors $\underline{\sigma}_m$, $\underline{\eta}_m$ based on the approximation that for the FGAHRS application, coning/sculling effects in $\underline{\sigma}_m$, $\underline{\eta}_m$ can be ignored – see [2, Section 3.4]. Similarly, assuming that scrolling effects are negligible for the FGAHRS application, position translation vector $\underline{\kappa}_m$ is calculated in Fig. 5a as a trapezoidal summation (integration) of $\underline{\upsilon}_k$ integrated acceleration measurements over the *m* cycle.

Having determined $\underline{\sigma}_m$, $\underline{\eta}_m$, $\underline{\kappa}_m$, the second block in Fig. 5a applies exact formulas from [1, Eqs. (7.3.3.2-19) and Sect. 19.1.3] to find corresponding changes in *B* frame attitude, velocity, position over the *m* cycle. The attitude change is represented by $C_{B_m}^{B_{m-1}}$, a direction cosine matrix that transforms vectors from their *B* frame components at the end of cycle *m* to their values at the end of the previous cycle (*m* –1). Velocity, position changes during rotation vector $\underline{\sigma}_m$ build-up over an *m* cycle, are represented in the *B* frame by $\Delta\underline{v}_{SF_m}^{B}$, $\Delta\underline{R}_{SF_m}^{B}$ induced by accelerometer measured "specific-force acceleration" (i.e., excluding gravity as accelerometers are prone to do).

In Fig. 5a blocks 3 - 5, the * notation is applied to the C_B^N, $\underline{v}_H^N$, $\Delta\underline{R}_{woLvH}^N$ integration parameters to identify their values following updates for the $C_{B_m}^{B_{m-1}}$, $\Delta\underline{v}_{SF_m}^{B}$, $\Delta\underline{R}_{SF_m}^{B}$ changes. The third block updates C_B^N for $C_{B_m}^{B_{m-1}}$ rotation from its $C_{B_{m-1}}^N$ value (at the end of cycle *m*-1) to $C^{*N}_{B_m}$. The fourth block in Fig. 5a transforms the calculated $\Delta\underline{v}_{SF_m}^{B}$, $\Delta\underline{R}_{SF_m}^{B}$ changes and measured magnetometer *m* cycle input vector $\underline{u}_{mag_m}^{B}$ into *N* frame coordinates $\Delta\underline{v}_{SF/H_m}^{N}$, $\Delta\underline{R}_{SF/H_m}^{N}$, $\underline{u}_{mag_m}^{N}$, paralleling the equivalent operations in Fig. 4. In accordance with the derivations in [1, Eqs. (7.3.3.2-19) & Sect. 19.1.3], exact $\Delta\underline{v}_{SF_m}^{B}$, $\Delta\underline{R}_{SF_m}^{B}$ transformations are executed using $C_{B_{m-1}}^N$ from the previous update cycle. In contrast, the $\underline{u}_{mag_m}^{B}$ transformation is achieved using the block 3 updated $C^{*N}_{B_m}$.

The last block in Fig. 5a uses $\Delta\underline{v}_{SF/H_m}^{N}$, $\Delta\underline{R}_{SF/H_m}^{N}$ to update $\underline{v}_H^N$, $\Delta\underline{R}_{woLv/H}^N$ for $\Delta\underline{v}_{SF/H_m}^{N}$, $\Delta\underline{R}_{SF/H_m}^{N}$ changes, from their values at the end of the previous *m* cycle into $\underline{v}^{*N}_{H_m}$, $\Delta\underline{R}^{*N}_{woLv/H_m}$ values at the end of the current *m* cycle. The $\Delta\underline{R}^{*N}_{woLv/H_m}$ update includes the integral of GPS horizontal velocity $\underline{v}_{GPS/H}^N$ over the *m* cycle (as in Fig. 4), using a digital trapezoidal integration algorithm. As in Fig. 4, horizontal position residual $\underline{R}{*}^{N}_{Resid/H_m}$ is then equated in block 5 to the updated $\Delta\underline{R}{*}^{N}_{woLv/H_m}$ corrected for lever arm motion, the lever arm correction based on the difference between C^{N}_{B0} and the block 3 updated $C{*}^{N}_{Bm}$ matrix. Lastly, $\underline{u}^{N}_{mag_m}$ from block 3 is used in block 5 to compute heading error residual ψ_{resid_m} using the formula provided in Fig. 4.

The primary computational accuracy in the FGAHRS algorithms stems from structuring Fig. 5a updating for IMU sensed inertial changes, with exact $C{*}^{N}_{Bm}$, $\underline{v}{*}^{N}_{H_m}$, $\Delta\underline{R}{*}^{N}_{woLv/H_m}$ updating algorithms. This also enables precision inertial software validation using simple exact validation simulators/procedures - e.g., [1, Sect. 11.2.2] for C^{N}_{B} validation under constant *B* and *N* angular rates, and [1, Sect. 11.2.3] for C^{N}_{B} , $\underline{v}^{N}_{H}$, $\Delta\underline{R}^{N}_{woLvH}$ validation under constant *B* frame angular-rates/accelerations under zero *N* frame rates. The $C{*}^{N}_{Bm}$, $\underline{v}{*}^{N}_{H_m}$, $\underline{R}{*}^{N}_{woLv/H_m}$, $\Delta\underline{R}{*}^{N}_{Resid/H_m}$, ψ_{resid_m} results from Fig. 5a are input to remaining *m* cycle computation blocks in Fig. 5b for FGAHRS feedback calculations and application.

The first block in Fig. 5b applies FGAHRS fixed gains $K_{\omega Bias_H}, K_{\omega Bias_\psi}, K_{\gamma_H}, K_{\gamma_\psi}$ to the $\Delta\underline{R}{*}^{N}_{Resid/H_m}$, ψ_{Resid_m} residuals to calculate the $\underline{\omega}^{N}_{FBm}$ angular rate feedback in Fig. 4 (including gyro bias estimation $\underline{\omega}^{N}_{BiasFBm}$ integrator update. The $\Delta\underline{v}^{N}_{H/FBm}$, $\Delta\underline{R}^{N}_{woLvFB/H_m}$ feedbacks for $\underline{v}^{N}_{H_m}$, $\underline{R}^{N}_{woLv/H_m}$ updating are calculated in Fig. 5a as increments of trapezoidal integration the *m* cycle the block 2 in Fig. 5b block 2. Similarly, the $\underline{\beta}^{N}_{FBm}$ angular feedback rotation increment in block 2 is computed as a trapezoidal integration increment of feedback the angular rate $\underline{\omega}^{N}_{FBm}$ determined in block 1.

The $\underline{\beta}^{N}_{FBm}$, $\Delta\underline{v}^{N}_{H/FBm}$, $\Delta\underline{R}^{N}_{woLvFB/H_m}$ feedback increments from block 2 are then used to update $C{*}^{N}_{Bm}$, $\underline{v}{*}^{N}_{H_m}$, $\underline{R}{*}^{N}_{woLv/H_m}$ from Fig. 5a. Block 2 uses $\underline{\beta}^{N}_{FBm}$ to update $C{*}^{N}_{Bm}$ into C^{N}_{Bm} , block 4 uses $\Delta\underline{v}^{N}_{H/FBm}$, $\Delta\underline{R}^{N}_{woLvFB/H_m}$ to update $\underline{v}{*}^{N}_{H_m}$, $\underline{R}{*}^{N}_{woLv/H_m}$ into $\underline{v}^{N}_{H_m}$, $\underline{R}^{N}_{woLv/H_m}$, completing the attitude, velocity, position residual updating operations for the *m* cycle.

Note in block 3 that based on [1, Sect. 7.1.1.3], an orthogonality/normality correction has been added following C^{N}_{Bm} updating to eliminate the possibility of E_{SYM} orthogonality/normality error buildup from computer round-off during continuous very long term operations (e.g., many days). The C_{Bm}^{N} attitude updating algorithms in Figs. 5a - 5b are exact and will retain exact orthogonality/normality if initialized that way. For an actual application, however, some orthogonality/normality error may gradually accumulate over time due to computational round-off. For the FGAHRS application, the effect will probably be negligible (using modern-day long-word-length floating-point processors). For safety (and because the associated computation is relatively trivial), the E_{SYM} measurement/application has been included in Fig. 5b block 3.

The last block in Fig. 5b provides the Eqs. (3) conversion formula for generating traditional FGAHRS roll, pitch, heading outputs ϕ, θ, ψ from C_{Bm}^{N}.

7. FGAHRS ERROR EQUATIONS

Analytically determining constant gain values for a specified stable FGAHRS response is facilitated by recognizing a fundamental characteristic of the ψ_{Resid}, $\underline{R}_{Resid_H}^{N}$ measurements in Fig. 4: When the $\underline{a}_{Accel}^{B}$, $\underline{l}^{B}$, $\underline{\omega}_{Gyro}^{B}$, $\underline{v}_{GPS_H}^{N}$, ψ_{Resid} signals are error free and the initial C_{B0}^{N}, $\underline{v}_{H_0}^{N}$ values are correct, ψ_{Resid}, $\underline{R}_{Resid_H}^{N}$ will be zero, hence, the resulting $\underline{\omega}_{FB}^{B}$, $\dot{\underline{v}}_{H_{FB}}^{N}$, $\Delta\dot{\underline{R}}_{woLv/H_{FB}}^{N}$ feedbacks will also be zero. Here's why.

The ψ_{Resid} equation in Fig. 4 was derived in Appendix C, representing the east component of earth's magnetic field vector $u_{mag_{east}}^{N}$ corrected for horizontal magnetic field variation θ_{dcln} from true north. With the θ_{dcln} correction, the computed horizontal magnetic field vector will be north, having zero east component (represented by ψ_{Resid}). Thus, under error free conditions, ψ_{Resid} will be zero as stipulated.

The proof for $\underline{R}_{Resid_H}^{N}$ is more involved. First, note that $\dot{\underline{R}}_{Resid_H}^{N}$, the derivative of $\underline{R}_{Resid_H}^{N}$ in Fig. 4, is given by $\dot{\underline{R}}_{Resid_H}^{N} = \dot{\underline{R}}_{woLv_H}^{N} - \frac{d}{dt}\left(C_B^N \underline{l}^B\right)_H$. Note also, that under zero error conditions, $\underline{v}_H^N$ will equal GPS horizontal velocity plus the IMU velocity relative the GPS antenna location, i.e., from (7), $\underline{v}_H^N = \underline{v}_{GPS_H}^N + \frac{d}{dt}\left(C_B^N \underline{l}^B\right)_H$. Thus, $\dot{\underline{R}}_{woLv_H}^{N}$, the $\Delta\underline{R}_{woLv_H}^{N}$ integrand in Fig. 4, will become $\dot{\underline{R}}_{woLv_H}^{N} = \frac{d}{dt}\left(C_B^N \underline{l}^B\right)_H - \Delta\dot{\underline{R}}_{woLv/H_{FB}}^{N}$, and substitution into the previous $\dot{\underline{R}}_{Resid_H}^{N}$ expression will find $\dot{\underline{R}}_{Resid_H}^{N} = -\Delta\dot{\underline{R}}_{woLv/H_{FB}}^{N}$. But from Fig. 4, $\Delta\dot{\underline{R}}_{woLv/H_{FB}}^{N} = K_R\,\underline{R}_{Resid_H}^{N}$. Thus, $\dot{\underline{R}}_{Resid_H}^{N} = -\,K_R\,\underline{R}_{Resid_H}^{N}$ or equivalently,

$\underline{\dot{R}}^N_{Resid\,H} + K_R\, \underline{R}^N_{Resid\,H} = 0$. This differential equation for $\underline{R}^N_{Resid\,H}$ shows that for positive K_R and for $\underline{R}^N_{Resid\,H}$ initially zero, $\underline{R}^N_{Resid\,H}$ will remain at zero.

The previous discussion demonstrated that under zero error conditions, ψ_{Resid}, $\underline{R}^N_{Resid\,H}$ will be zero, hence, the $\underline{\omega}^B_{FB}$, $\underline{\dot{v}}^N_{H\,FB}$, $\Delta\underline{\dot{R}}^N_{woLv/H\,FB}$ feedback corrections derived from them will also be zero. Thus, Fig. 4 operations would proceed as if there was no feedback, accurately propagating the FGAHRS solution without error. Conversely, if there are FGAHRS error sources, ψ_{Resid}, $\underline{R}^N_{Resid\,H}$ will only measure the error source effects. Thus, an equivalent set of FGAHRS error equations can be used to assess accuracy under all conditions, with or without error mechanisms. This finding provides the basis for analytically deriving FGAHRS fixed gain values for stable closed-loop performance (in Section 7) based on the FGAHRS computational error equations.

7.1 FGAHRS OPEN-LOOP ERROR EQUATIONS

Processing Fig. 4 equations under open-loop (zero feedback) conditions propagates into the following differential error equation form as derived in Appendix A and summarized in (A-14):

$$
\begin{gathered}
\underline{\dot{\gamma}}^N_H = -\left(C^N_B\, \delta\underline{\omega}^B_{Gyro}\right)_H \qquad \dot{\gamma}^N_{Down} = -\left(C^N_B \delta\underline{\omega}^B_{Gyro}\right)_{Down} \\
\delta\underline{\dot{v}}^N_H \approx \left(C^N_B \delta\underline{a}^B_{Accel}\right)_H + g\, \underline{\gamma}^N_H \times \underline{u}^N_{Down} - \gamma^N_{Down}\, \underline{u}^N_{Down} \times \underline{a}^N_{Accel\,H} \\
\delta\Delta\underline{\dot{R}}^N_{woLv\,H} = \delta\underline{v}^N_H - \delta\underline{v}^N_{GPS\,H} \\
\delta\underline{R}^N_{Resid\,H} = \delta\Delta\underline{R}^N_{woLv\,H} - \left(C^N_B\, \delta\underline{l}^B\right)_H + \left(C^N_B\, \delta\underline{l}^B\right)_{H\,0}
\end{gathered}
\tag{12}
$$

In (12), $\underline{\gamma}^N_H$, γ^N_{Down} are horizontal (*H*) and vertically downward (*Down*) angular errors in the C^N_B matrix (treating the errors as a small angular rotation vector of the *N* frame from its nominal horizontal/vertical orientation), $\delta\underline{\omega}^B_{Gyro}$ is the IMU gyro output error vector in the *B* frame, $\delta\underline{v}^N_H$ is the horizontal velocity error, $\delta\underline{a}^B_{Accel}$ is the IMU accelerometer output error vector in the *B* frame, *g* is gravity magnitude (assumed constant), $\delta\Delta\underline{R}^N_{woLv\,H}$ is the lever-arm-uncompensated horizontal position change error, $\delta\underline{R}^N_{Resid\,H}$ is the lever-arm compensated horizontal position change error, δ indicates the error in the identified parameters, and 0 indicates the error parameter value at time $t = 0$.

7.2 FGAHRS CLOSED-LOOP ERROR EQUATIONS (INCLUDING FEEDBACK)

Including the feedback (FB) terms in Fig. 4 for closed-loop operation, converts open-loop Eqs. (12) into the following closed-loop error model derived in Appendix B and summarized in (B-12):

$$
\begin{aligned}
\delta \dot{\underline{\omega}}_{BiasFB_H}^{N} &= - K_{\omega Bias_H}\, \underline{u}_{Down}^{N} \times \delta \Delta \underline{R}_{woLv_H}^{N} \\
&\quad + K_{\omega Bias_H}\, \underline{u}_{Down}^{N} \times \left[\left(C_B^N \delta \underline{l}^B \right)_H - \left(C_B^N \delta \underline{l}^B \right)_{H_0} \right] \\
\dot{\underline{\gamma}}_H^N &= - \left(C_B^N\, \delta \underline{\omega}_{Gyro}^{B} \right)_H + \delta \underline{\omega}_{BiasFB_H}^{N} - K_{\gamma_H}\, \underline{u}_{Down}^{N} \times \delta \Delta \underline{R}_{woLv_H}^{N} \\
&\quad + K_{\gamma_H}\, \underline{u}_{Down}^{N} \times \left[\left(C_B^N \delta \underline{l}^B \right)_H - \left(C_B^N \delta \underline{l}^B \right)_{H_0} \right]
\end{aligned} \tag{13}
$$

$$
\begin{aligned}
\delta \dot{\underline{v}}_H^N &\approx \left(C_B^N \delta \underline{a}_{Accel}^{B} \right)_H - K_v\, \delta \Delta \underline{R}_{woLv_H}^{N} + g\, \underline{\gamma}_H^N \times \underline{u}_{Down}^{N} - \gamma_{Down}^{N}\, \underline{u}_{Down}^{N} \times \underline{a}_{Accel_H}^{N} \\
&\quad + K_v \left[\left(C_B^N\, \delta \underline{l}^B \right)_H - \left(C_B^N\, \delta \underline{l}^B \right)_{H_0} \right] \\
\delta \Delta \dot{\underline{R}}_{woLv_H}^{N} &= \delta \underline{v}_H^N - K_R\, \delta \Delta \underline{R}_{woLv_H}^{N} - \delta \underline{v}_{GPS_H}^{N} + K_R \left[\left(C_B^N \delta \underline{l}^B \right)_H - \left(C_B^N \delta \underline{l}^B \right)_{H_0} \right]
\end{aligned} \tag{14}
$$

$$
\begin{aligned}
\delta \dot{\omega}_{BiasFB_{Down}}^{N} &= - K_{\omega Bias_\psi} \left[\gamma_{dwn}^{N} - \tan \theta_{incln}\, \gamma_{nrth}^{N} - K_{\omega Bias_\psi} \frac{\underline{u}_{east}^{N} \cdot \left(C_B^N\, \delta \underline{u}_{mag}^{B} \right)}{u_{mag_{nrth}}^{N}} \right] \\
\dot{\gamma}_{Down}^{N} &= - \underline{u}_{Down}^{N} \cdot \left(C_B^N\, \delta \underline{\omega}_{Gyro}^{B} \right) \\
&\quad - K_{\gamma_\psi} \left[\gamma_{dwn}^{N} - \tan \theta_{incln}\, \gamma_{nrth}^{N} - K_{\gamma_\psi} \frac{\underline{u}_{east}^{N} \cdot \left(C_B^N\, \delta \underline{u}_{mag}^{B} \right)}{u_{mag_{nrth}}^{N}} \right] + \delta \omega_{BiasFB_{Down}}^{N}
\end{aligned} \tag{15}
$$

In (13) – (15), $\underline{u}_x^B$ is a unit vector along the strapdown IMU B frame x axis.

Eqs. (13) – (14) are closed-loop differential error equations for Fig. 4 FGAHRS horizontal channel computations of attitude, velocity, position change using GPS horizontal velocity derived feedback corrections. Eqs. (15) are closed-loop error equations for the FGAHRS vertical (heading) channel computation using magnetometer derived heading error feedback. These equations match the open-loop error equations in (12), plus added feedback through 4 horizontal channel gains K_R, K_v, K_{γ_H}, $K_{\omega Bias_H}$ and 2 heading channel gains $K_{\gamma_\psi}, K_{\omega Bias_\psi}$. When the gains are zero, (13) – (15) revert to their pure open-loop inertial form in (12) whose error term definitions also apply for (13) – (15).

The form of (13) – (15) facilitates determination of gain values to achieve specified horizontal and heading channel time response characteristics.

8.0 FGAHRS FIXED GAIN DETERMINATION

8.1 HORIZONTAL CHANNEL GAINS

The horizontal channel error equations in (13) – (14) summarize as follows:

$$\begin{aligned}
\delta\dot{\underline{\omega}}_{\omega FB_H}^{N} &= -K_{\omega Bias_H}\,\underline{u}_{Down}^{N}\times\delta\Delta\underline{R}_{woLv_H}^{N}+\cdots \\
\dot{\underline{\gamma}}_{H}^{N} &= \delta\underline{\omega}_{BiasFB_H}^{N}-K_{\gamma_H}\,\underline{u}_{Down}^{N}\times\delta\Delta\underline{R}_{woLv_H}^{N}+\cdots \\
\delta\dot{\underline{v}}_{H}^{N} &= g\,\underline{\gamma}_{H}^{N}\times\underline{u}_{Down}^{N}-\gamma_{Down}^{N}\,\underline{u}_{Down}^{N}\times\underline{a}_{Accel_H}^{N}-K_{v}\,\delta\Delta\underline{R}_{woLv_H}^{N}+\cdots \\
&\approx -g\,\underline{u}_{Down}^{N}\times\underline{\gamma}_{H}^{N}-K_{v}\,\delta\Delta\underline{R}_{woLv_H}^{N}+\cdots \\
\delta\Delta\dot{\underline{R}}_{woLv_H}^{N} &= \delta\underline{v}_{H}^{N}-K_{R}\,\delta\Delta\underline{R}_{woLv_H}^{N}+\cdots
\end{aligned} \tag{16}$$

where $\cdots$ refers to other input error terms. Note in (16) that $\gamma_{Down}^{N}\,\underline{u}_{Down}^{N}\times\underline{a}_{Accel_H}^{N}$ has been dropped as negligible in the $\delta\dot{\underline{v}}_{H}^{N}$ equation (based on the assumption that it is small compared to the $g\,\underline{\gamma}_{H}^{N}\times\underline{u}_{Down}^{N}$ term). An alternate approach might be to consider analytically cancelling (rather than dropping) this term by adding a $\gamma_{Down}^{N}\,\underline{u}_{Down}^{N}\times\underline{a}_{Accel_H}^{N}$ cross-coupling correction to the $\dot{\underline{v}}_{H_{FB}}^{N}$ velocity rate feedback in Fig. 4 block 3. The γ_{Down}^{N} term for cross-coupling correction would be the negative of the ψ_{Resid} magnetometer measurement in block 3 - see (C-10) and its derivation in Appendix C. However, using ψ_{Resid} in this manner would then introduce a $\tan\theta_{incln}\,\gamma_{nrth}^{N}\left(\underline{u}_{Down}^{N}\times\underline{a}_{Accel_H}^{N}\right)$ error into the block 3 $\underline{v}_{H}^{N}$ integrand. Under high magnetic field inclination angles (i.e., at high or low latitudes), the $\tan\theta_{incln}$ effect could overshadow the cross-coupling correction benefit.

Taking the first, second, and third derivatives of the last three expressions in (16) finds

$$\begin{aligned}
\dot{\delta\underline{\omega}}_{\omega FB_H}^{N} &= -K_{\omega Bias_H}\,\underline{u}_{Down}^{N}\times\delta\Delta\underline{R}_{woLv_H}^{N}+\cdots \\
\ddot{\underline{\gamma}}_{H}^{N} &= \dot{\delta\underline{\omega}}_{\omega FB_H}^{N}-K_{\gamma_H}\,\underline{u}_{Down}^{N}\times\delta\dot{\underline{R}}_{woLv_H}^{N}\cdots \\
\delta\dddot{\underline{v}}_{H}^{N} &- g\,\underline{u}_{Down}^{N}\times\ddot{\underline{\gamma}}_{H}^{N}-K_{v}\,\delta\ddot{\underline{R}}_{woLv_H}^{N}+\cdots \\
\delta\Delta\ddddot{\underline{R}}_{woLv_H}^{N} &= \delta\dddot{\underline{v}}_{H}^{N}-K_{R}\,\delta\dddot{\underline{R}}_{woLv_H}^{N}+\cdots
\end{aligned} \tag{17}$$

Substituting the first of (17) into the second, that result into the third, and that result into the fourth then finds

$$
\begin{aligned}
&\delta\dot{\underline{\omega}}_{\omega FB_H}^{N} = -K_{\omega Bias_H}\,\underline{u}_{Down}^{N}\times\delta\Delta\underline{R}_{woLv_H}^{N} + \cdots \\[2ex]
&\ddot{\underline{\gamma}}_{H}^{N} = \delta\dot{\underline{\omega}}_{BiasFB_H}^{N} - K_{\gamma_H}\,\underline{u}_{Down}^{N}\times\delta\Delta\dot{\underline{R}}_{woLv_H}^{N}\cdots \\
&= -K_{\omega Bias_H}\,\underline{u}_{Down}^{N}\times\delta\Delta\underline{R}_{woLv_H}^{N} - K_{\gamma_H}\,\underline{u}_{Down}^{N}\times\delta\Delta\dot{\underline{R}}_{woLv_H}^{N} + \cdots \\[2ex]
&\delta\dddot{\underline{v}}_{H}^{N} = -g\,\underline{u}_{Down}^{N}\times\ddot{\underline{\gamma}}_{H}^{N} - K_{v}\,\delta\Delta\ddot{\underline{R}}_{woLv_H}^{N} + \cdots \\
&= -g\,\underline{u}_{Down}^{N}\times\left[-\underline{u}_{Down}^{N}\times\left(K_{\omega Bias_H}\,\delta\Delta\underline{R}_{woLv_H}^{N} + K_{\gamma_H}\,\delta\Delta\dot{\underline{R}}_{woLv_H}^{N}\right)\right] \\
&\qquad - K_{v}\,\delta\Delta\ddot{\underline{R}}_{woLv_H}^{N} + \cdots \\
&= -K_{v}\,\delta\Delta\ddot{\underline{R}}_{woLv_H}^{N} - g\left(K_{Bias_H}\,\delta\Delta\underline{R}_{woLv_H}^{N} + K_{\gamma_H}\,\delta\Delta\dot{\underline{R}}_{woLv_H}^{N}\right) + \cdots \\[2ex]
&\delta\Delta\ddddot{\underline{R}}_{woLv_H}^{N} = \delta\dddot{\underline{v}}_{H}^{N} - K_{R}\,\delta\Delta\dddot{\underline{R}}_{woLv_H}^{N} + \cdots \\
&= -K_{v}\,\delta\Delta\ddot{\underline{R}}_{woLv_H}^{N} - g\left(K_{Bias_H}\,\delta\Delta\underline{R}_{woLv_H}^{N} + K_{\gamma_H}\,\delta\Delta\dot{\underline{R}}_{woLv_H}^{N}\right) \\
&\qquad - K_{R}\,\delta\Delta\dddot{\underline{R}}_{woLv_H}^{N} + \cdots
\end{aligned}
\tag{18}
$$

or with rearrangement:

$$
\delta\Delta\ddddot{\underline{R}}_{woLv_H}^{N} + K_{R}\,\delta\Delta\dddot{\underline{R}}_{woLv_H}^{N} + K_{v}\,\delta\Delta\ddot{\underline{R}}_{woLv_H}^{N} + K_{\gamma_H}\,g\,\delta\Delta\dot{\underline{R}}_{woLv_H}^{N} + K_{\omega Bias_\psi}\,g\,\delta\Delta\underline{R}_{woLv_H}^{N} = \cdots \tag{19}
$$

Eq. (19) is a linear differential equation with constant coefficients having Laplace transform

$$
\left(s^4 + s^3 K_R + s^2 K_v + s\,g K_{\gamma_H} + g K_{\omega Bias_H}\right)\mathcal{L}\left(\delta\Delta\underline{R}_{woLv_H}^{N}\right) = \mathcal{L}(\cdots) \tag{20}
$$

where s is the Laplace transform frequency parameter, and $\mathcal{L}(\;)$ indicates the Laplace transform of ( ). The bracketed term in (20) is the characteristic root equation for Eqs. (18). By equating it to a desired response characteristic, the individual gains can be determined, e.g., setting each of the four roots to have a $1/\tau_H$ characteristic response frequency, where τ_H is the desired characteristic response time constant. Setting the bracketed term in (20) to $\left(s+\frac{1}{\tau_H}\right)^4$ then obtains

$$
\begin{aligned}
s^4 + s^3 K_R + s^2 K_v + s\, g K_{\gamma_H} + g K_{\omega Bias_H} &= \left(s + \frac{1}{\tau_H} \right)^4 \\
&= s^4 + s^3 \frac{4}{\tau_H} + s^2 \frac{6}{\tau_H^2} + s\, \frac{4}{\tau_H^3} + g\, \frac{1}{\tau_H^4}
\end{aligned} \tag{21}
$$

Equating coefficients of equal powers of s finds for the AHRS horizontal channel gains:

$$
K_R = \frac{4}{\tau_H} \qquad K_v = \frac{6}{\tau_H^2} \qquad K_{\gamma_H} = \frac{4}{g\, \tau_H^3} \qquad K_{\omega Bias_\psi} = \frac{1}{g\, \tau_H^4} \tag{22}
$$

8.2 VERTICAL (HEADING) CHANNEL GAINS

Following the same procedure leading to the (22) horizontal gains, the heading channel gains are determined from differential equations in (15):

$$
\begin{aligned}
\delta\dot{\omega}^N_{BiasFB_{Down}} &= - K_{\omega Bias_\psi} \left(\gamma^N_{dwn} - \tan\theta_{incln}\, \gamma^N_{nrth} \right) + \cdots \\
&\approx - K_{\omega Bias_\psi}\, \gamma^N_{Down} + \cdots \\
\\
\dot{\gamma}^N_{Down} &= \delta\omega^N_{\omega FB_{Down}} - K_{\gamma_\psi} \left(\gamma^N_{dwn} - \tan\theta_{incln}\, \gamma^N_{nrth} \right) + \cdots \\
&\approx - K_{\gamma_\psi}\, \gamma^N_{Down} + \delta\omega^N_{BiasFB_{Down}} + \cdots
\end{aligned} \tag{23}
$$

The approximation in (23) of dropping the $\tan\theta_{incln}\, \gamma^N_{nrth}$ term in (15) is based on the assumption that it will not significantly impact closed-loop performance. This step was necessary to produce a set of linear constant coefficient error equations in (23) as the basis for closed-loop fixed gain determination.

Differentiating $\dot{\gamma}^N_{Down}$ in (23) and substituting $\dot{\gamma}^N_{Down}$ from the first expression in (23) obtains

$$
\ddot{\gamma}^N_{Down} \approx - K_{\gamma_\psi}\, \dot{\gamma}^N_{Down} + \delta\dot{\omega}^N_{\omega FB_{Down}} + \cdots = - K_{\gamma_\psi}\, \dot{\gamma}^N_{Down} - K_{\omega Bias_\psi}\, \gamma^N_{Down} + \cdots \tag{24}
$$

Upon rearrangement, (24) becomes

$$
\ddot{\gamma}^N_{Down} + K_{\gamma_\psi}\, \dot{\gamma}^N_{Down} + K_{\omega Bias_\psi}\, \gamma^N_{Down} = \cdots \tag{25}
$$

Eq. (25) is a linear differential equation with constant coefficients whose Laplace transform is

$$\left(s^2 + s\,K_{\gamma_\psi} + K_{\omega Bias_\psi}\right)\mathcal{L}\left(\gamma^N_{Down}\right) = -\,\mathcal{L}\left(\cdots\right) \tag{26}$$

Equating the bracketed characteristic root expression in (26) to the equivalent of two roots, each with a characteristic response frequency of $1/\tau_\psi$ (for a τ_ψ characteristic response time constant), finds

$$s^2 + s\,K_{\gamma_\psi} + K_{\omega Bias_\psi} = \left(s + \frac{1}{\tau_\psi}\right)^2 = s^2 + s\,\frac{2}{\tau_\psi} + \frac{1}{\tau_\psi^2} \tag{27}$$

The heading channel gains are then obtained by equating coefficients of like powers of *s*:

$$K_{\gamma_\psi} = \frac{2}{\tau_\psi} \qquad K_{\omega Bias_\psi} = \frac{1}{\tau_\psi^2} \tag{28}$$

9. FGAHRS AUTOMATIC GYRO BIAS CALIBRATION MODE

The advantage of including the $\underline{\omega}^N_{BiasFB}$ gyro bias estimators in the FGAHRS Fig. 4 (and Fig. 3) feedback structure is that it allows gyro bias to be estimated and corrected (compensated) as part of normal in-use operations. The method is to transform $\underline{\omega}^N_{BiasFB}$ from the *N* frame to the *B* frame using the inverse (transpose) of C^N_B. However, before this is executed, sufficient time must elapse for heading rate transients to decay in the FGAHRS closed-loop structure. The approach is to verify (by test) that heading rate remains small over the transient decay time of the FGAHRS computations (e.g., the larger of the horizontal and heading loop transient decay times), then issuing the compensation reset command to correct the existing gyro bias compensation by an $\underline{\omega}^N_{BiasFB}$ amount (while simultaneously resetting $\underline{\omega}^N_{BiasFB}$ to zero). (Note: For the fourth order horizontal FGAHRS loop with gains set to the equivalent of four sequential first order responses of time constant τ_H, the combined response time is $4\,\tau_H$ and for a "3 sigma" transient wait period, the wait time would be $12\,\tau_H$. Similarly, for the second order FGAHRS heading loop (with gains set to the equivalent of two sequential first order responses of time constant τ_ψ), the combined response time is $2\,\tau_\psi$ and for a "3 sigma" wait period, the transient wait time would be $6\,\tau_\psi$.) The following illustrates how the auto gyro bias correction operation might be implemented within the FGAHRS Fig. 5b algorithm structure.

$$\Delta t_{\psi_m} = \Delta t_{\psi_{m-1}} + T_m$$

$$\cos\psi_m = \frac{C_{11_m}}{\sqrt{C_{11_m}^2 + C_{21_m}^2}} \qquad \sin\psi_m = \frac{C_{21_m}}{\sqrt{C_{11_m}^2 + C_{21_m}^2}}$$

$$\Delta\psi_{Tst} = \sin\left(\psi - \psi_{Smp}\right) = \sin\psi_m \cos\psi_{Smp} - \cos\psi_m \sin\psi_{Smp}$$

(29)

If $\left(\left|\Delta\psi_{Tst}\right| > \Delta\psi_{Max}\right)$ Then:

$\Delta t_{\psi_m} = 0 \qquad \sin\psi_{Smp} = \sin\psi_m \qquad \cos\psi_{Smp} = \cos\psi_m$

Else If $\left(\Delta t_{\psi_m} > T_{AHRS_{Trns}}\right)$ Then:

$\Delta t_{\psi_m} = 0$

$\underline{\omega}_{BiasCmp}(+) = \underline{\omega}_{BiasCmp}(-) + \left(C_B^N\right)^T \underline{\omega}_{BiasFB}^N$

$\underline{\omega}_{BiasFB}^N = 0$

End If

In (29), Δt_{ψ_m} is the time interval since the last reset when the heading change remained less than the prescribed limit $\Delta\psi_{Max}$, $\Delta\psi_{Tst}$ is the measurement of heading change since the last Δt_{ψ_m} reset, $\sin\psi_m$, $\cos\psi_m$ are the sine and cosine of heading extracted from C_B^N (based on using $C*_B^N$ in Fig. 5a), $\sin\psi_{Smp}$, $\cos\psi_{Smp}$ are sampled values of $\sin\psi_m$, $\cos\psi_m$ at Δt_{ψ_m} reset, $T_{AHRS_{Trns}}$ is the time interval for AHRS closed-loop computation transients to decay (e.g., 3 times the response time), $\underline{\omega}_{BiasFB}^N$ is the estimated *N* frame gyro bias in computed Fig. 5b block 1, $\underline{\omega}_{BiasCmp}(-)$ is the IMU gyro bias compensation vector before $(-)$ the update, and $\underline{\omega}_{BiasCmp}(+)$ is the IMU gyro bias compensation vector after (+) the update. Auto Gyro Calibration Eqs. (29) would be executed following the $C*_B^N$ update in Fig. 5a block 3. Gyro bias compensation $\underline{\omega}_{BiasCmp}$ in (29) would then be applied continuously to the IMU gyro output generated rotation vector in Fig. 5a block 1.

$$\underline{\sigma}_m(+) = \underline{\sigma}_m - \underline{\omega}_{BiasCmp} T_m \qquad (30)$$

where $\underline{\sigma}_m(+)$ is the compensated rotation vector. The $\underline{\sigma}_m(+)$ compensated $\underline{\sigma}_m$ would be used in place of the uncompensated $\underline{\sigma}_m$ in Fig. 5a following the block 1 compensation correction.

10. HANDLING MAGNETOMETER DERIVED CROSS-COUPLING DYNAMICS

A fundamental problem using a strapdown magnetometer triad for FGAHRS heading referencing, is the presence of a vertical of earth's magnetic field vector component in the $\underline{u}_{mag_m}^{B}$ measurement (manifested in magnetic field inclination angle θ_{incln}). At very high or low latitudes, the θ_{incln} angle approaches 90 degrees, the corresponding north magnetic field component $u_{mag/nrth_m}^{N}$ approaches zero, and the ψ_{resid_m} heading error measurement in Fig. 5a block 5 approaches a singularity condition. The result translates into the Fig. 5b attitude error feedback rate $\underline{\omega}_{FB_m}^{N}$, increasing heading error with closer θ_{incln} proximity to 90 degrees.

The magnetometer cross-coupling effect arises from using the FGAHRS computed C_B^N matrix (and its attendant errors) in the $\underline{u}_{mag_m}^{N}$ transformation operation in Fig. 5a block 4, and subsequent generation of the ψ_{resid_m} heading error measurement in block 5. The computed ψ_{resid_m} is applied through heading loop gains K_{γ_ψ}, $K_{\omega Bias_\psi}$ to generate the Fig. 5b block 1 attitude feedback rate $\underline{\omega}_{FB_m}^{N}$ used in Fig. 5b blocks 2 and 3 for updating C_B^N. The overall closed-loop result is that C_B^N attitude error γ_{nrth}^{N} (around the north axis) couples into C_B^N heading error γ_{Down}^{N}. The effect appears analytically in $\dot{\gamma}_{Down}^{N}$ closed-loop error Eqs. (15) as $\tan\theta_{incln}\,\gamma_{nrth}^{N}$. Under horizontal acceleration, the horizontal γ_{nrth}^{N} induced γ_{Down}^{N} heading error will then couple back into the (14) horizontal control loops, potentially producing instability.

Two approaches can be considered for mitigation: 1) Reducing the heading loop feedback control gains ($K_{\omega Bias_\psi}$ and K_{γ_ψ}), or 2) Reducing the γ_{nrth}^{N} tilt error. Reducing heading loop gains increases the time for transients to settle, thereby increasing the time requirement for sufficient straight-line navigation for gyro bias auto calibration (see Section 9). Reducing the γ_{nrth}^{N} tilt error is a more complicated operation, necessitating the ability to deduce and reduce γ_{nrth}^{N} based on available FGAHRS measurements. Since γ_{nrth}^{N} is generated by several FGAHRS error sources (most notably horizontal accelerometer error), in-use estimation/correction generally involves a sophisticated estimation process. The classical method of dealing with such issues has been through use of a Kalman filter.

Proper operation of a Kalman filter requires reasonably accurate models for the error effects being estimated, both deterministic error models, and error model uncertainty characteristics - as manifested in the classical covariance matrix (or equivalent) imbedded within Kalman estimation. Unfortunately, for commercially available MEMS inertial sensors (gyros/accelerometers), statistical error models are not readily available since their system use has not been generally required. MEMS sensor statistical uncertainty is further complicated by the multiplicity of commercial MEMS manufacturers with differing design configurations and associated error characteristics. An alternative to Kalman filtering is estimation based on classical least squares error averaging, a simpler averaging technique that does not require error statistics in its analytical formulation.

In the past, least squares averaging has not commonly been applied to multiple error source problems due, in part, to past memory and throughput limitations in real-time navigation micro-processors (and the popularity of Kalman filtering in modern applications). Such limitations are no longer a problem for modern-day micro-processors. As such, least squares estimation can now be a considered a viable option for a commercial MEMS-based AHRS application to estimate and correct errors induced by strapdown magnetometer heading measurements at high latitudes. A subsequent article will describe how least squares estimation can be applied to the FGAHRS configuration discussed in this article.

11. PERFORMANCE ANALYSIS

11.1 DIGITAL TRAJECTORY GENERATOR SIMULATION PROGRAM

To evaluate the accuracy of various FGAHRS configurations, a simulation program was developed for generating IMU, magnetometer, and GPS velocity outputs with a corresponding exact attitude, velocity, position solution under user specified trajectory conditions. The simulation defines the trajectory as a series of user specified heading turns (each for a specified time period, heading rate, and forward acceleration change) coupled with user specified 3-dimensional linear and angular oscillations (each at specified frequency, amplitude, start and end time along the trajectory). The simulation is constructed as a set of exact closed-form analytical equations that can be programmed into a subroutine for output at any specified time point. Simulation outputs are exact ("error-free") attitude, velocity, position navigation data at a specified time instant, and a corresponding set of error-free strapdown gyro/accelerometer signals that would be output from an error-free strapdown IMU following the trajectory. Integration of the gyro/accelerometer outputs using exact strapdown integration algorithms will yield a navigation solution identical to that provided by the simulator. The simulator is designed to generate trajectories representative of surface (at sea or on land) vehicle motion characteristics.

The subprogram that interfaces the trajectory generator with simulated FGAHRS computational algorithms, generates corresponding GPS velocity and magnetometer output signals, adding user specified errors to these and to the simulated IMU sensor signals for output. A subsequent article will describe the simulator, deriving the equations for programming into a digital simulation. For the performance evaluation described in this article, the following describes the trajectory generator simulation configuration.

The trajectory begins at time t=0 at zero velocity and 90 deg heading. The segment turn profile in Table 1 is executed during the trajectory by the simulated vehicle's rotation center:

Table 1 – Trajectory Turn Profile

Segment Number	Start Time	Time Duration	Heading Change	Velocity Change	Segment End Heading	Segment End Velocity
1	0 Sec	33 Sec	0 deg	0 fps	90 deg	0 fps
2	33 sec	10 sec	0 deg	20 fps	90 deg	20 fps
3	43 sec	4.5 sec	90 deg	0 fps	180 deg	20 fps
4	47.5 sec	20 sec	0 deg	0 fps	180 deg	20 fps
5	67.5 sec	10.25 sec	-55 deg	20 fps	125 deg	40 fps
6	77.75 sec	20.5 sec	0 deg	0 fps	125 deg	40 fps
7	98.25 sec	5 sec	-55 deg	0 fps	70 deg	40 fps
8	103.25 sec	20 sec	0 deg	0 fps	70 deg	40 fps
9	123.25 sec	5 sec	90 deg	0 fps	160 deg	40 fps
10	128.25 sec	20 sec	0 deg	0 fps	160 deg	40 fps
11	148.25 sec	5 sec	-55 deg	0 fps	105 deg	40 fps
12	153.25 sec	26.75 sec	0 deg	0 fps	105 deg	40 fps

For the duration of the trajectory, the following linear oscillations of the rotation center and angular oscillations around the rotation center were present:

Angular Oscillations			Linear Oscillations		
B-Frame Axis	Peak-To Peak Amplitude	Frequency	N-Frame Axis	Peak-To-Peak Amplitude	Frequency
Roll (x)	20 Deg	0.4 Hz	North (x)	1 Ft	0.2 Hz
Pitch (y)	20 Deg	0.15 Hz	East (y)	1 Ft	0.15 Hz
Heading (z)	6 Deg	0.35 Hz	Down (z)	2 Ft	0.35 Hz

The FGAHRS IMU vehicle location during the trajectory was simulated at a user specified vector distance from the ship's rotation center of 5 ft fore (forward), 3 ft port-side (left), 7.5 ft upward, producing rotation generated accelerometer outputs that added to the center-of-rotation acceleration.

Figs. 6a –6*l* depict the resulting reference trajectory attitude, velocity, position history and corresponding error-free strapdown IMU gyro/accelerometer inputs.

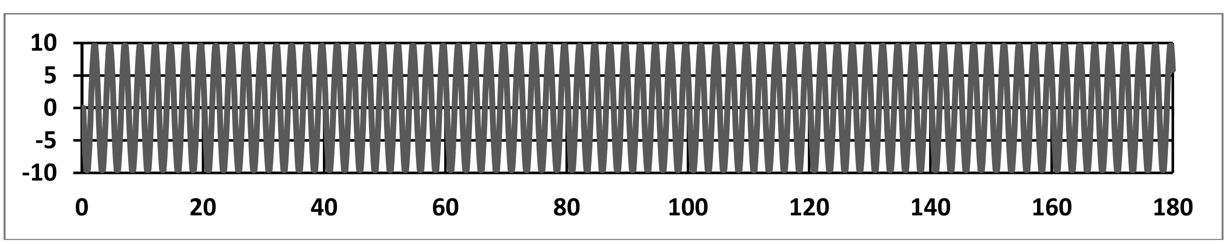

Fig. 6a - Roll (deg) vs. Time (sec)

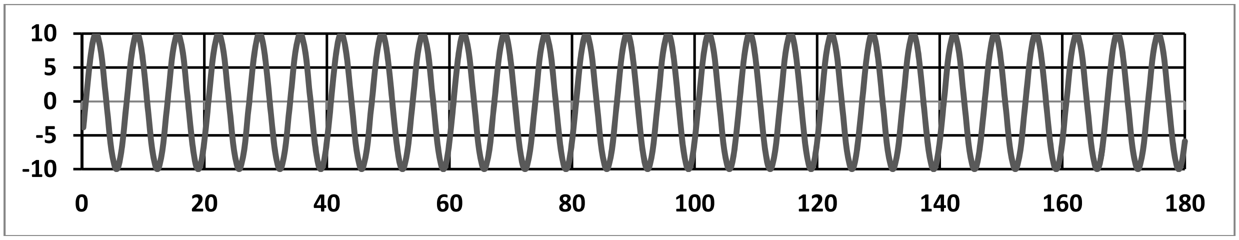

Fig. 6b - Pitch (deg) vs. Time (sec)

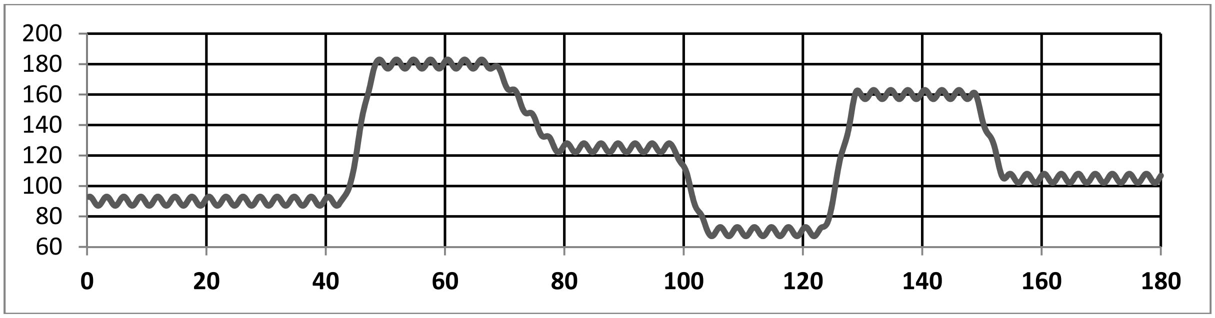

Fig. 6c - Heading (deg) vs. Time (sec)

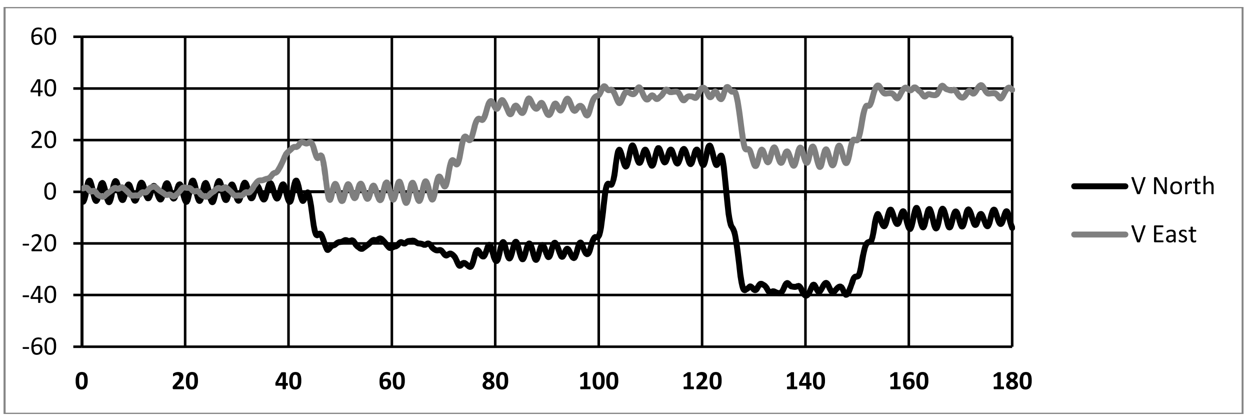

Fig. 6d - Horizontal Velocity (fps) vs. Time (sec)

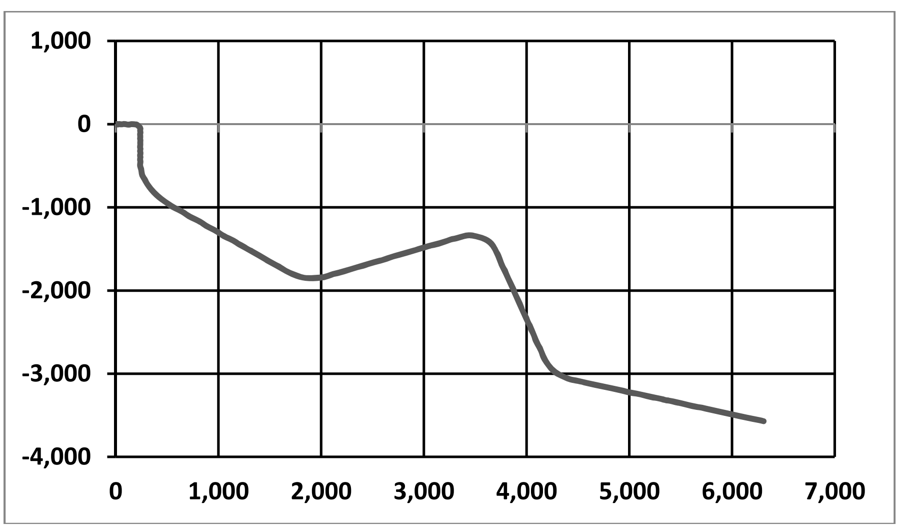

Fig. 6e – East Distance ("y" ordinate axis - ft) vs. North Distance ("x" abscissa axis - ft)

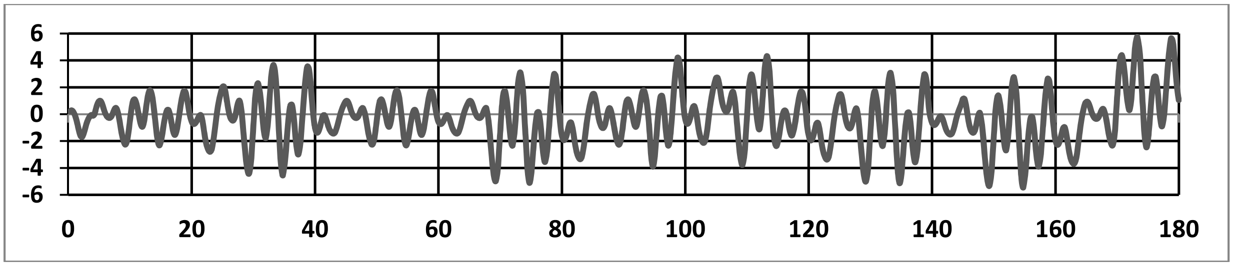

Fig. 6f - Distance Down (ft) vs. Time (sec)

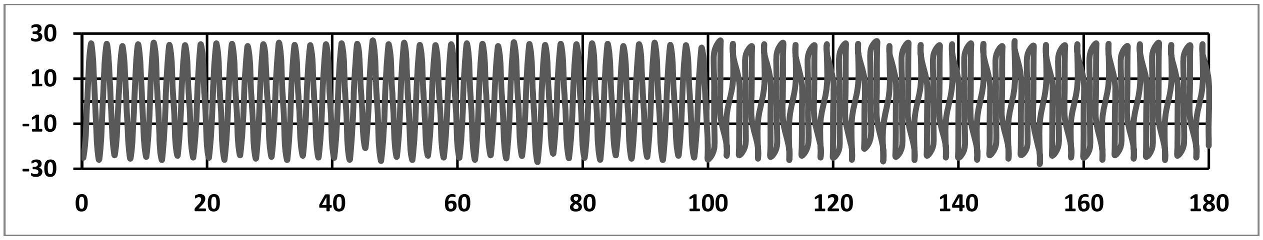

Fig. 6g - X Gyro Input (deg/sec) vs. Time (sec)

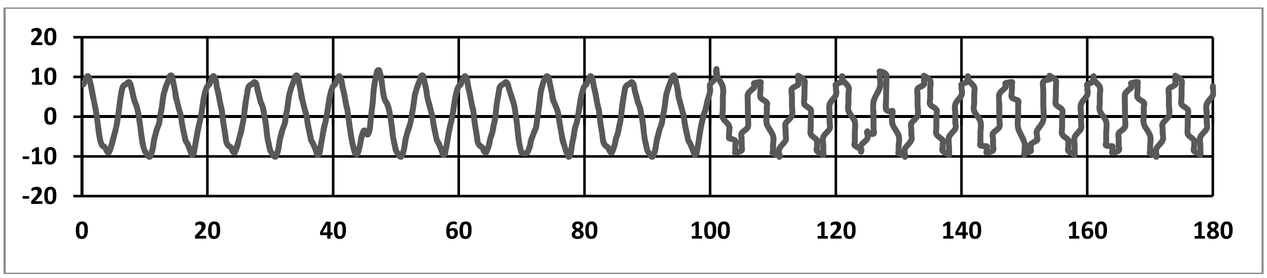

Fig. 6h - Y Gyro Input (deg/sec) vs. Time (sec)

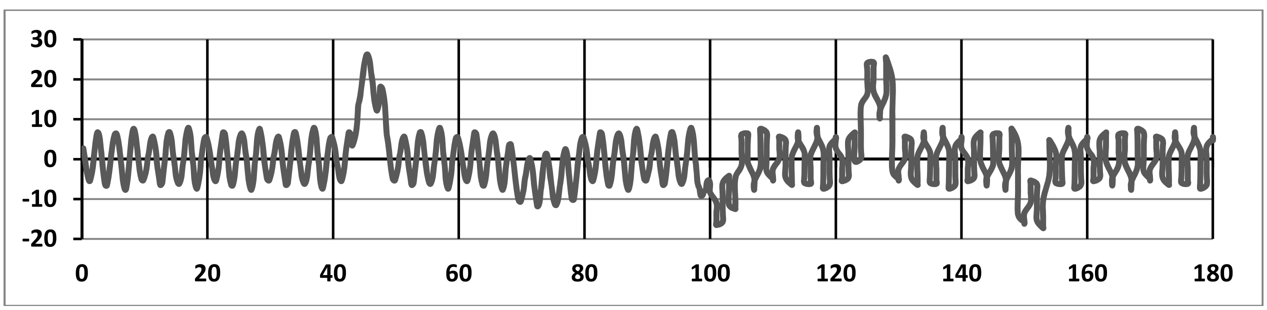

Fig. 6i - Z Gyro Input (deg/sec) vs. Time (sec)

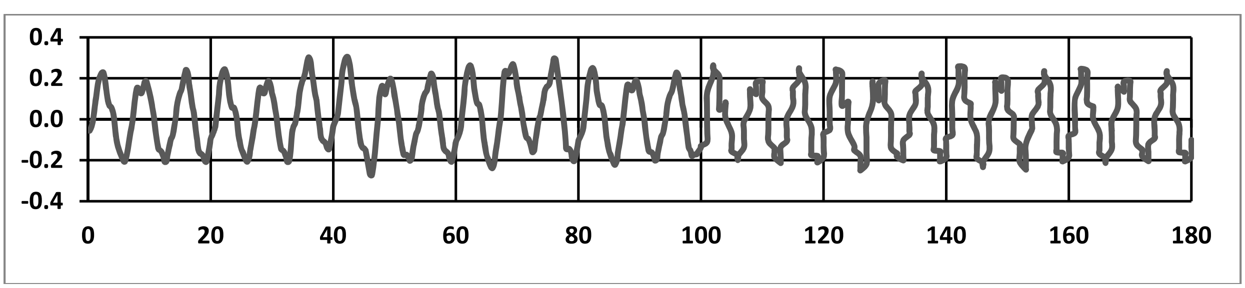

Fig. 6j - X Accelerometer Input (gs) vs. Time (sec)

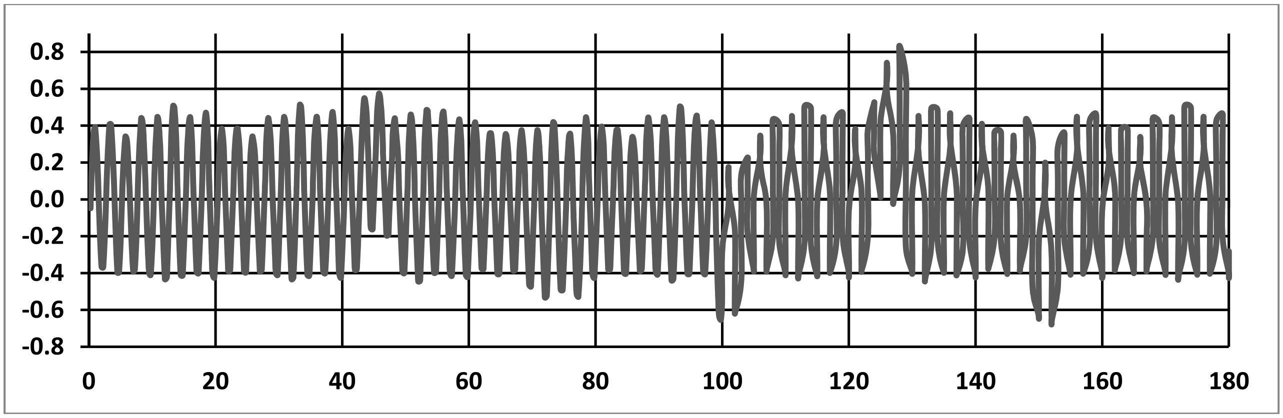

Fig. 6k - Y Accelerometer Input (gs) vs. Time (sec)

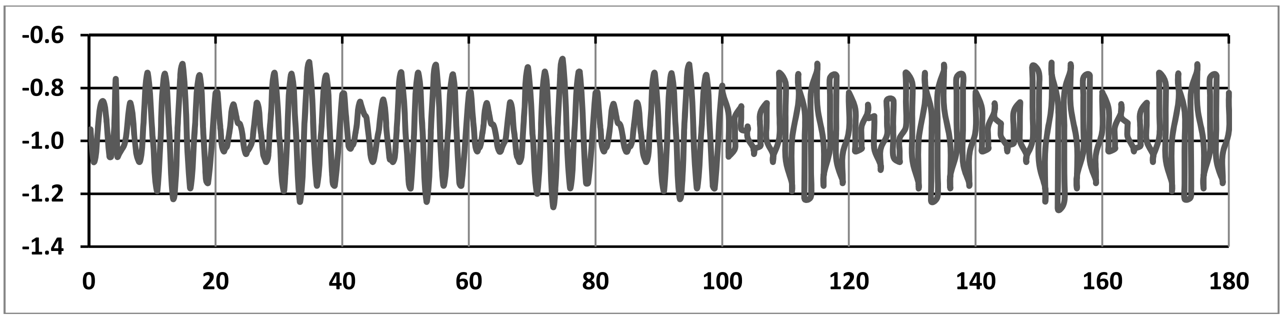

Fig. 6*l* - Z Accelerometer Input (gs) vs. Time (sec)

11.2 FGAHRS COMPUTATIONAL CONFIGURATION DURING PERFORMANCE EVALUATION

During performance evaluation, the FGAHRS algorithms were initialized using the process described in Section 5. Following initialization, the Section 6 FGAHRS computational algorithms were executed at a 100 hz update rate (T_m = 0.01 sec update time interval). The Auto Gyro Bias Compensation operation in Section 9 was not engaged except as a variation to illustrate its effectiveness (described in Section 11.6.3).

During performance evaluation, the following values were used for the FGAHRS computation algorithm constants:

Update Cycle Time (T_m) = 0.01 sec
Horizontal Loop Characteristic Time Constant (τ_H) = 1 sec
Vertical (Heading) Loop Characteristic Time Constant (τ_ψ) = 6 sec

From (22) and (28) the associated FGAHRS feedback loop gains became

$$K_R = 4 \sec^{-1} \quad K_v = 6 \sec^{-2} \quad K_{\gamma_H} = 0.124\, g^{-1} \sec^{-3} \quad K_{\omega Bias_\psi} = 0.0311\, g^{-1} \sec^{-4}$$

$K_{\gamma_\psi} = 0.333 \sec^{-1} \qquad K_{\omega Bias_\psi} = 0.0278 \sec^{-2}$

11.3 NOMINAL FGAHRS PERFORMANCE EVALUATION

Nominal FGAHRS performance is defined as response under zero error conditions, including coarse initialization followed by FGAHRS closed-loop operation using the Section 6 computation algorithms. Nominal FGAHRS conditions include operation at 30 deg N latitude and 93 deg W longitude, the longitude corresponding to maximum earth magnetic field inclination from vertical (with increasing latitude). At 30 deg latitude, the magnetic field inclination angle from vertical is 58.94 deg. It was assumed for nominal performance evaluation that the magnetic field declination angle (magnetic variation) was completely compensated within the FGAHRS software. Under nominal conditions, auto gyro bias compensation was disabled.

Figs. 7a – 7d depict simulated nominal FGAHRS roll, pitch, heading errors generated under the Figs. 6a – 6*l* trajectory conditions. Fig 7a shows the errors from trajectory start time $t = 0$ to trajectory end at $t = 180$ seconds. Fig. 7b shows the first 20 seconds of Fig 7a to provide detail of attitude convergence from the Section 5 applied initialization process. Figs. 7c – 7d show the Fig. 7a data from $t = 20$ to 180 seconds and from $t = 60$ to 180 seconds (using an expanded vertical scale to more clearly define converged attitude error magnitudes).

Fig 7b shows that attitude initialization convergence begins with a heading error of -12 deg. The large initial heading error arises from the large initial attitude error (order of 10 deg) around the north axis coupling into the magnetometer derived heading error measurement through the tangent of the local magnetic inclination angle - see (B-3) of Appendix B. The large north attitude error arises from the coarse attitude initialization process in Section 5.1 that approximates initial roll/pitch attitude to be zero, while "actual" (simulated) roll/pitch was oscillating at ± 10 deg amplitudes.

Figs. 7c – 7d demonstrate that following initialization transient convergence, nominal FGAHRS attitude errors are essentially zero throughout the remaining Section 11.1 dynamic trajectory, including sustained horizontal acceleration periods in Table 1 of 10 seconds duration for Segment 2 (starting at $t = 33$ seconds) and of 10.25 seconds duration for Segment 5 (starting at $t = 67.5$ seconds). The residual errors remaining in Fig. 7d are primarily caused by approximations in the FGAHRS Fig. 5a block 1 computation algorithms - equating the rotation/velocity-translation vectors ($\underline{\sigma}_m$, $\underline{\eta}_m$) to increments of integrated strapdown IMU gyro/accelerometer outputs (without adding coning/sculling compensation).

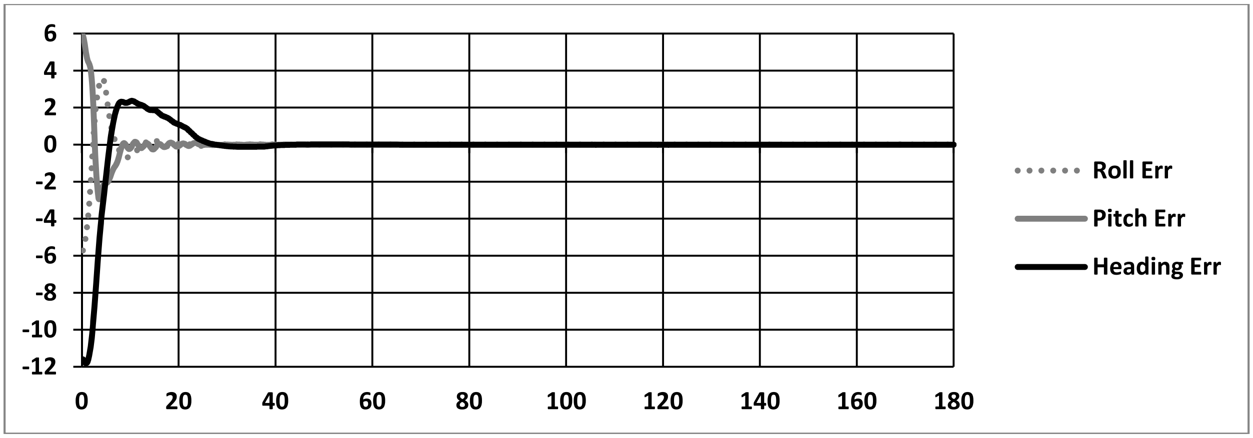

Fig. 7a - Roll, Pitch, Heading Error (deg) vs. Time (sec)
Nominal Conditions (Zero Errors)

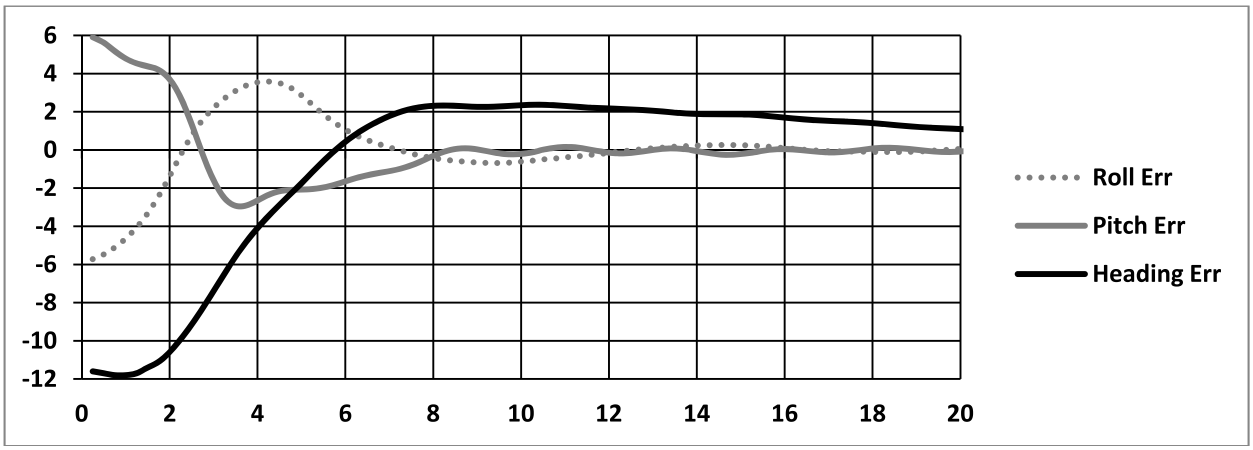

Fig. 7b - Roll, Pitch, Heading Error (deg) vs. Time (sec)
Nominal Conditions (Zero Errors) – First 20 Seconds

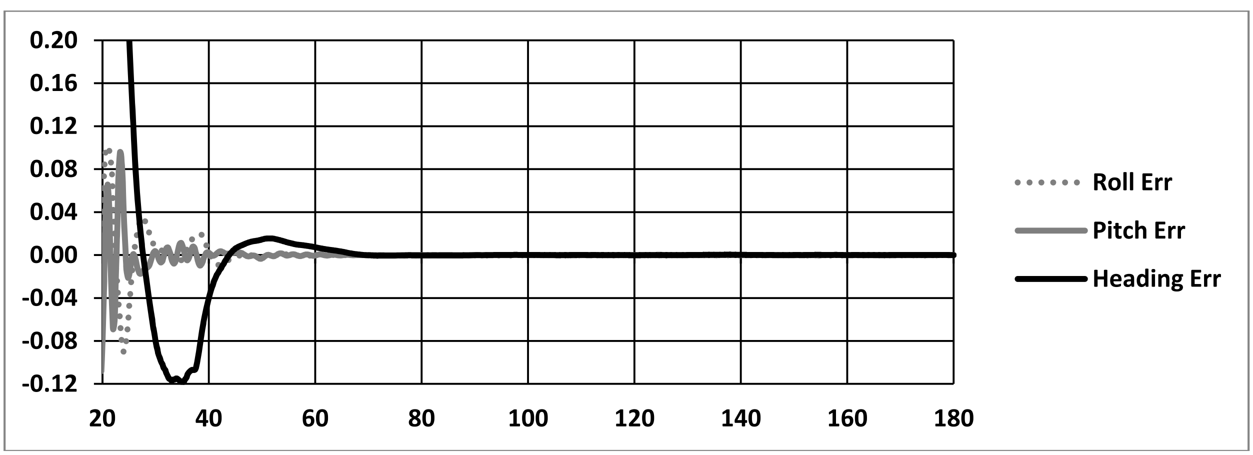

Fig. 7c - Roll, Pitch, Heading Error (deg) vs. Time (sec) – Expanded Attitude Error Scale
Nominal Conditions (Zero Errors) – 20 To 180 Seconds

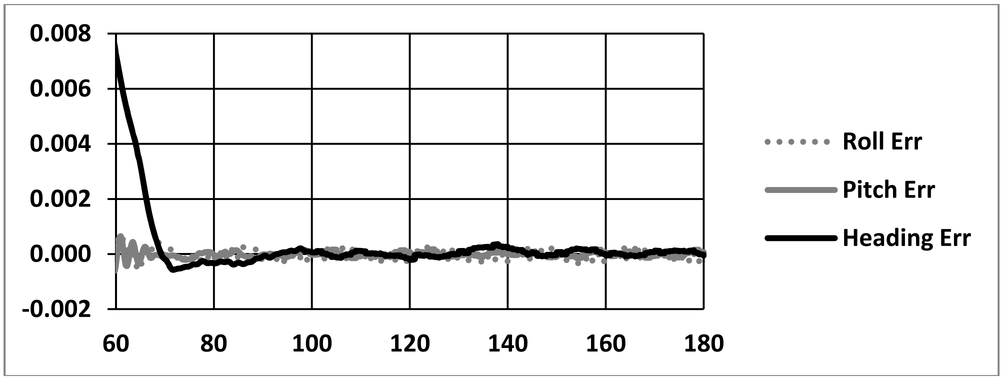

Fig. 7d - Roll, Pitch, Heading Error (deg) vs. Time (sec) – Expanded Attitude Error Scale
Nominal Conditions (Zero Errors) – 60 To 180 Seconds

11.3.1 <u>Nominal FGAHRS Vs Conventional AHRS Performance For Zero Magnetic Field Inclination Angle</u>

Figs. 8a – 8d compare FGAHRS nominal (error free) performance with what would be achieved using the nominal Fig. 3 conventional AHRS using integrated horizontal acceleration ("velocity") <u>without GPS velocity correction</u> for horizontal attitude tilt feedback, and magnetometer feedback for heading error control. The FGAHRS configuration used in the investigation was as described in Fig. 4, with magnetometer feedback for closed-loop heading error control, and with <u>GPS velocity correction</u> included within the integrated horizontal velocity ("position residual") horizontal closed-loop feedback structure.

The conventional AHRS horizontal feedback configuration in Fig. 3 can be classified as a "third order" closed-loop structure (three interconnected attitude, velocity, gyro bias estimation integrators undergoing closed-loop control). The AHRS heading control loop was configured to match the Fig. 3 AHRS "second order" magnetometer aiding approach (for attitude and gyro bias estimation), using a characteristic time constant (τ_ψ) set to 1.5 of the horizontal feedback control loop characteristic time constant (τ_H) – To equalize the resulting AHRS control feedback third order horizontal and second order heading loop response times (i.e., 2 × τ_ψ = 3 × τ_H).

The FGAHRS horizontal feedback configuration in Fig. 4 can be classified as a "fourth order" closed-loop structure because of the four interconnected integrators (attitude, velocity, integrated velocity, gyro bias estimation) undergoing closed-loop control. The FGAHRS heading control loop was configured to match the Fig. 4 FGAHRS "second order" magnetometer aiding approach (for attitude and gyro bias estimation). Section 11.3 defines the baseline values for the baseline FGAHRS characteristic time constants (τ_H and τ_ψ) used for performance evaluation.

To clarify the FGAHRS versus conventional strapdown AHRS comparison, the magnetic field inclination angle was set to zero (to eliminate the associated north tilt coupling into heading effect - See Section 10. It was also assumed that the magnetic field declination angle (magnetic variation) was completely compensated within the AHRS and FGAHRS software. Both the FGAHRS and conventional AHRS configurations used the initialization process in Section 5, an exception being that for the conventional AHRS, initial velocity was set to zero (because GPS velocity was not available for AHRS initialization - as it was in Section 5.2 for the FGAHRS). Both the FGAHRS and AHRS simulation tests used the Section 11.1 simulated trajectory for performance evaluation.

The Fig. 8a result shows that roll, pitch errors for the AHRS configuration were on the order of 6 deg when the τ_H characteristic time constant was set to 10 seconds (the equivalent of a 30 second "one sigma" response time for the associated third order feedback control loop). Note the initialization convergence characteristics in Fig. 8a during the first 33 seconds of AHRS operation (under static trajectory conditions – see Segment 1 of Table 1). For τ_H increased to 20 seconds (60 second one sigma response time), the AHRS roll, pitch errors in Fig. 8b reduced to 2 deg (but for a doubling of the initial transient response time compared with Fig. 8a). However, when the trajectory velocity was increased from 40 to 60 fps (i.e., from 27 to 41 statute miles per hour), AHRS roll, pitch errors in Fig. 8c increased to 4 deg. (The velocity increase was achieved by increasing the Segment 2 velocity change in Table 1 from 20 to 40 fps.)

The results in Figs. 8a – 8c were what was expected from a conventional AHRS, demonstrating its roll, pitch error susceptibility to horizontal acceleration (either from velocity magnitude change in the forward direction or from velocity directional change generating lateral centripetal acceleration during high angular rate turning). Decreasing the horizontal feedback gain reduces this error effect, but at sacrifice of response time and increased attitude error buildup from gyro bias following maneuver turns. The latter effect becomes feedback configuration limiting for an AHRS using a commercial grade MEMS IMU where gyro bias on the order of 1 deg/sec can be expected (e.g., for a 20 second τ_H time constant setting as in Figs. 8b – 8c, 1 deg/sec gyro bias can quickly build to 20 deg attitude error before its growth becomes restrained by feedback). Use of the Section 9 auto gyro bias compensation could also be used for the conventional AHRS to partially compensate large gyro bias errors. However, longer delay time would then be required at constant heading (see Section 9) for low gain feedback transient decay. For τ_H = 20 seconds as in Figs. 8b and 8c, a 2 sigma transient delay time allowance for the third order horizontal control loop would be $3 \times 20 \times 2 = 120$ seconds.

In contrast with Fig. 8c for the conventional AHRS, Fig. 8d demonstrates the performance characteristics of the FGAHRS under the same zero error conditions used for the AHRS in Fig. 8c. Compared with the conventional AHRS 4 deg errors in Fig. 8c, Fig. 8d demonstrates that following a much shorter initialization transient time decay period, the FGAHRS roll, pitch, heading errors are imperceptibly small.

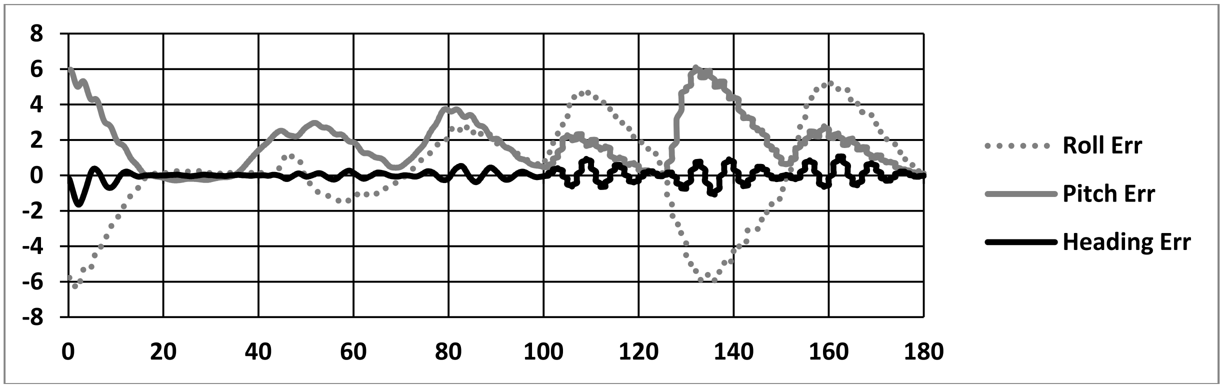

Fig. 8a – Conventional Strapdown AHRS Roll, Pitch, Heading Error (deg) vs. Time (sec)
Using Velocity Feedback Without GPS Velocity Correction
Characteristic Horizontal Loop Response Time τ_H = 10 Seconds
Nominal Conditions (Zero Errors) With Zero Magnetic Field Inclination

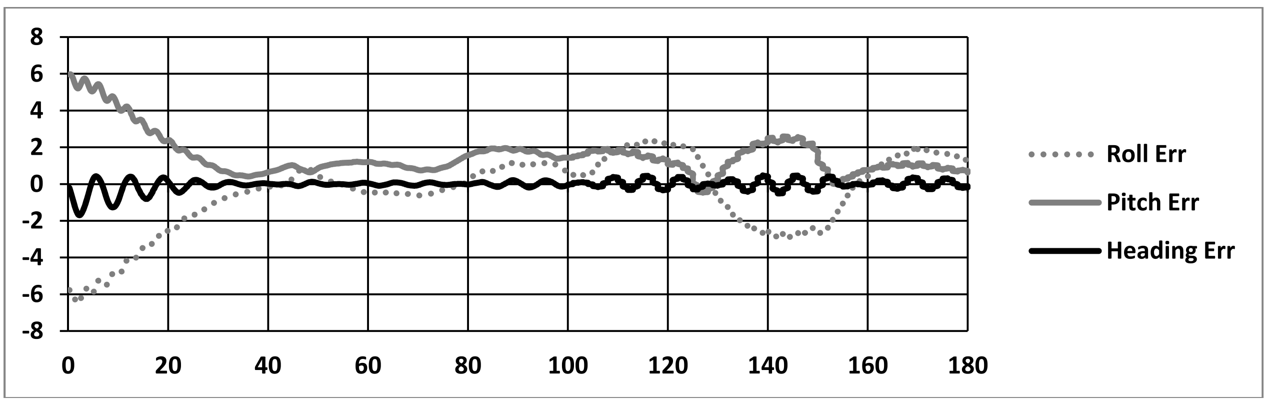

Fig. 8b – Conventional Strapdown AHRS Roll, Pitch, Heading Error (deg) vs. Time (sec)
Using Velocity Feedback Without GPS Velocity Correction
Characteristic Horizontal Loop Response Time τ_H = 20 Seconds
Nominal Conditions (Zero Errors) With Zero Magnetic Field Inclination

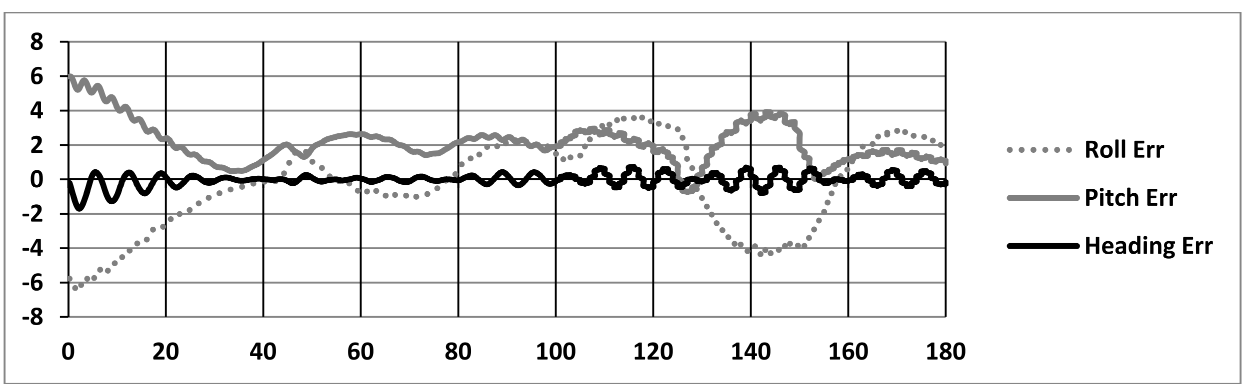

Fig. 8c – Conventional Strapdown AHRS Roll, Pitch, Heading Error (deg) vs. Time (sec)
Using Velocity Feedback Without GPS Velocity Correction
Characteristic Horizontal Loop Response Time τ_H = 20 Seconds
Nominal Conditions (Zero Errors) But With Zero Magnetic Field Inclination
First Velocity Change (Segment 2) Increased From 20 To 40 fps

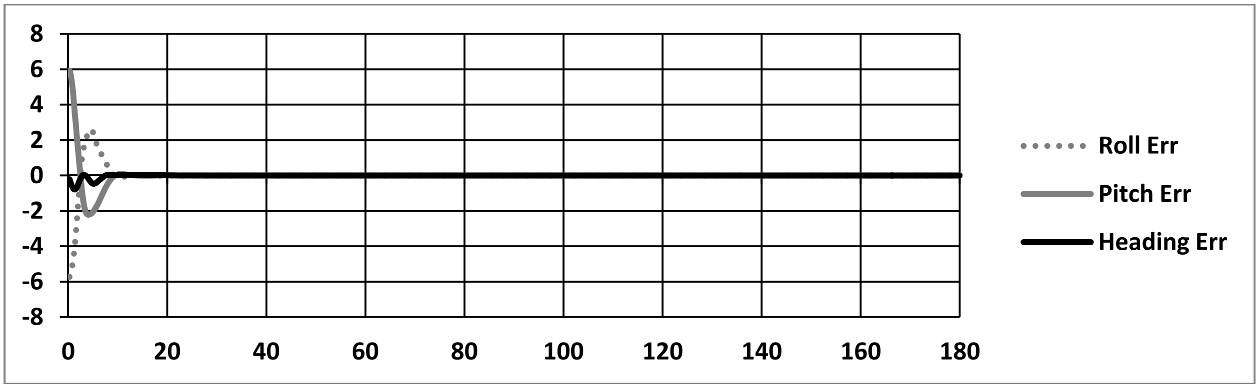

Fig. 8d – Strapdown FGAHRS Roll, Pitch, Heading Error (deg) vs. Time (sec)
Using Integrated Velocity Feedback With GPS Velocity Correction
Characteristic Horizontal Loop Response Time τ_H = 1 Second
Nominal Conditions (Zero Errors) With Zero Magnetic Field Inclination
First Velocity Change (Segment 2) Increased From 20 To 40 fps

11.4 BASELINE FGAHRS COMPONENT ERROR VALUES

Baseline FGAHRS performance is defined as response under typical error conditions, including coarse initialization followed by FGAHRS closed-loop operation using the Section 6 computation algorithms. The following IMU, GPS, and magnetometer error source values were used during baseline performance evaluation. Variations from some of these values were also included as part of the performance evaluation process (described in Section 11.6).

11.4.1 IMU Sensor Errors: IMU gyro/accelerometer errors used during baseline performance analysis were as shown in Table 2.

Table 2 – Baseline IMU Inertial Sensor Errors

X Gyro Bias: 0.1 deg/sec Y Gyro Bias: 0.1 deg/sec Z Gyro Bias: 0.1 deg/sec
X Gyro Misalignment into Y: 1.0 deg X Gyro Misalignment into Z: -1.3 deg
Y Gyro Misalignment into Z: -0.75 deg Y Gyro Misalignment into X: -1.0 deg
Z Gyro Misalignment into X: -1.3 deg Z Gyro Misalignment into Y: -0.9 deg
X Gyro Scale Factor Error: 0.15 % Y Gyro Scale Factor Error: -0.09 %
Z Gyro Scale Factor Error: 0.12 %
X, Y, Z Gyro Random Walk Noise: 2 deg/sqrt(hr) = 0.033 deg/sqrt(sec)
= 0.033 (deg/sec)/sqrt(hz) = negligible ≈ 0

X Accel Bias: 3.0 milli-g Y Accel Bias: 3.0 milli-g Z Accel Bias: -0.9 milli-g
X Accel Misalignment into Y: 1.0 deg X Accel Misalignment into Z: -1.0 deg
Y Accel Misalignment into Z: 1.3 deg Y Accel Misalignment into X: -1.0 deg
Z Accel Misalignment into X: -0.8 deg Z Accel Misalignment into Y: -1.2 deg
X Accel Scale Factor Error: 0.12 % Y Accel Scale Factor Error: 0.15 %
Z Accel Scale Factor Error: -0.13 %
X, Y, Z Accel Random Walk Noise: 0.3 milli-g-sec/sqrt(sec)
= 0.3 milli-g/sqrt(hz) = negligible ≈ 0

The 0.1 deg/sec gyro bias and 3 milli-g accelerometer bias figures in Table 1 are based on prior FGAHRS in-use operation using the Section 9 auto sensor compensation processes. An FGAHRS auto bias compensation process is also available for the accelerometers based on least squares error estimation theory (as will be described in a planned future article).

Commercially available MEMS gyros/accelerometer accuracies are on the order of 1 deg/sec and 10 milli-gs. These would have been in-use calibrated down to the 0.1 deg/sec, 3 milli-g levels in Table 1 using the previously described procedures. Variation performance simulation results to be shown in Sections 11.6.1 - 11.6.2 demonstrate performance at the uncompensated 1 deg/sec, 10 milli-g levels.

11.4.2 GPS Errors: The GPS velocity errors were defined to be zero for performance evaluation described in this article. Parallel simulation studies have demonstrated that GPS velocity errors of 2 fps have virtually no impact on baseline FGAHRS attitude accuracy.

11.4.3 Magnetometer Errors: Magnetometer heading misalignment relative to the IMU (or equivalently, stray magnetic field bias) was set at approximately 1 deg for baseline performance evaluation. The impact of a 5 deg IMU-to-magnetometer misalignment was also assessed (described in Section 11.6.1). The effect of magnetometer-to-IMU heading misalignment was simulated by adding 5 deg changes to the gyro/accelerometer 1,2 and 2,1 misalignment coefficients in Table 2, with the 1,2 changes set to the negative of the 2,1 changes.

11.4.4 Lever Arm Compensation Errors: GPS-Receiver-to-IMU lever arm compensation errors were included during baseline FGAHRS performance evaluation:

X forward axis GPS-Receiver-to-IMU lever arm compensation error = 0.5 ft
Y starboard (right) axis GPS-Receiver-to-IMU lever arm compensation error = 0.5 ft
Z axis (downward) GPS-Receiver-to-IMU lever arm compensation error = 0 ft

The impact of 10 ft in X, 5 ft in Y variations from these values were included as part of performance evaluation (described in Section 11.6.1).

11.5 BASELINE FGAHRS PERFORMANCE EVALUATION

Baseline FGAHRS conditions are defined as containing Section 11.4 errors operating at 30 deg N latitude and 93 deg W longitude, the longitude corresponding to maximum earth magnetic field inclination from vertical (with increasing latitude). At 30 deg latitude, the magnetic field inclination angle from vertical is 58.94 deg. It was assumed for the baseline and variation performance studies that the magnetic field declination (magnetic variation) was completely compensated within the FGAHRS software. Under the baseline simulation conditions, auto gyro bias compensation was disabled.

Figs. 9a – 9c depict the baseline FGAHRS roll, pitch, heading errors generated under Figs. 6a – 6*l* trajectory conditions. Fig. 9a shows the errors from trajectory start time $t = 0$ to trajectory end a $t = 180$ sec. Fig. 9b shows the first 20 seconds of Fig. 4a to provide detail of attitude convergence from the Section 5 applied initialization process. Fig. 9c shows the Fig. 6a data from 20 to 180 seconds following coarse alignment convergence (using an expanded vertical scale to more clearly distinguish the roll, pitch, heading errors).

As with the nominal (error free) performance results in Fig. 7a – 7b of Section 11.3, Figs.9a - 9b shows that baseline attitude initialization convergence performance begins from a large heading error of -12 deg (induced by the applied Section 5.1 coarse attitude initialization process – See Section 11.3 for further explanation). Fig. 9c shows that following initialization convergence, FGAHRS roll, pitch, heading accuracy (under the Section 11.4 applied baseline error conditions), then remains within 1 deg under the dynamic trajectory conditions depicted in Figs. 6a – 6*l*.

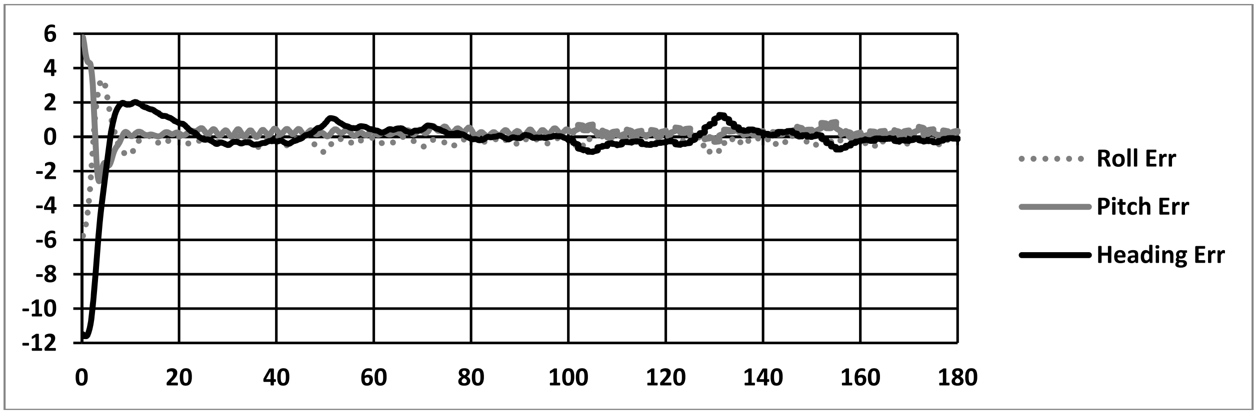

Fig. 9a - Roll, Pitch, Heading Error (deg) vs. Time (sec)
Baseline Error Conditions

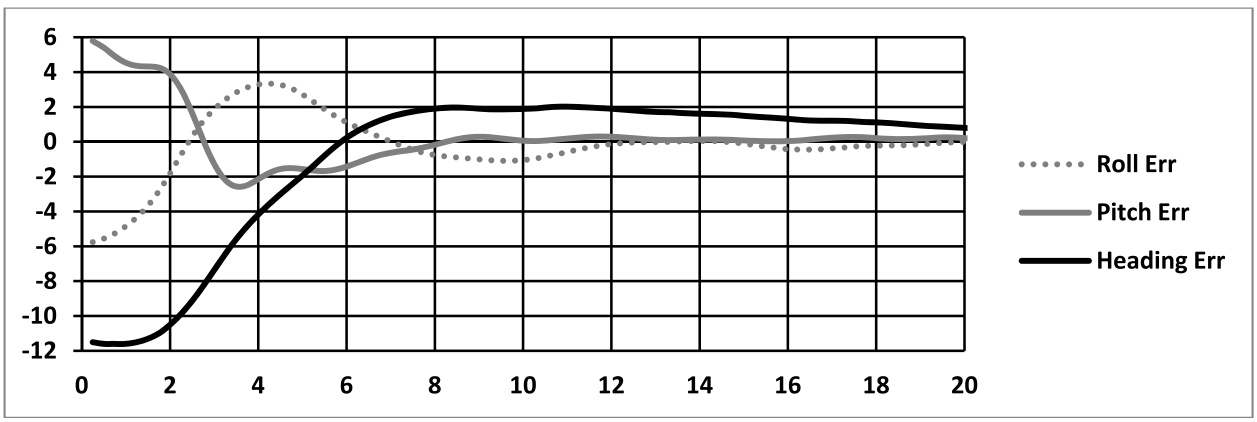

Fig. 9b - Roll, Pitch, Heading Error (deg) vs. Time (sec)
Baseline Error Conditions – First 20 Seconds

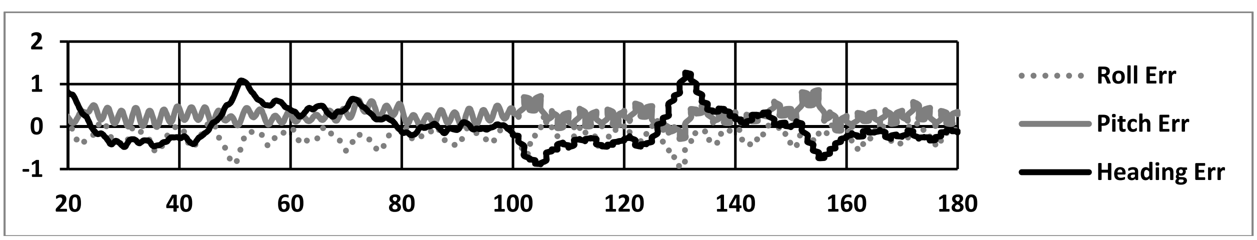

Fig. 9c - Roll, Pitch, Heading Error (deg) vs. Time (sec)
Baseline Error Conditions – 20 To 180 Seconds

11.6 FGAHRS PERFORMANCE UNDER VARIATIONS FROM THE BASELINE

Simulation studies have shown that the largest errors impacting FGAHRS accuracy are GPS-antenna-to-IMU lever arm compensation error, magnetometer-to-IMU heading misalignment (or the equivalent stray magnetic field bias), “horizontal” accelerometer bias, and gyro bias. The Section 11.4 baseline values for these parameters were based on having them previously calibrated, during FGAHRS installation calibration of lever arm and misalignment errors, and by FGAHRS in-use auto compensation engagement for the accelerometer and gyro biases.

11.6.1 Error Sources Requiring Calibration During FGAHRS Installation

GPS antenna-to-IMU lever arms and magnetometer-to-IMU heading alignment would be calibrated in the user vehicle during FGAHRS installation, with the expectation that results will remain valid (stable) during future installed system use. Installation calibration applies least squares estimation (built into the FGAHRS software) during a brief approximately straight accelerating trajectory (to be described in a forthcoming article). The baseline 0.5 ft lever arm errors of Section 11.4.4 and 1 deg magnetometer heading misalignment error of Section 11.4.3 represent values following installation calibration. Figs. 10 and 11 show the effect of operation with 10 and 5 ft uncalibrated lever arms and an uncalibrated heading alignment error of 5 deg. Comparison with baseline Fig. 9c FGAHRS performance shows a substantial increase in heading error under non-calibration conditions, illustrating the need for installation calibration.

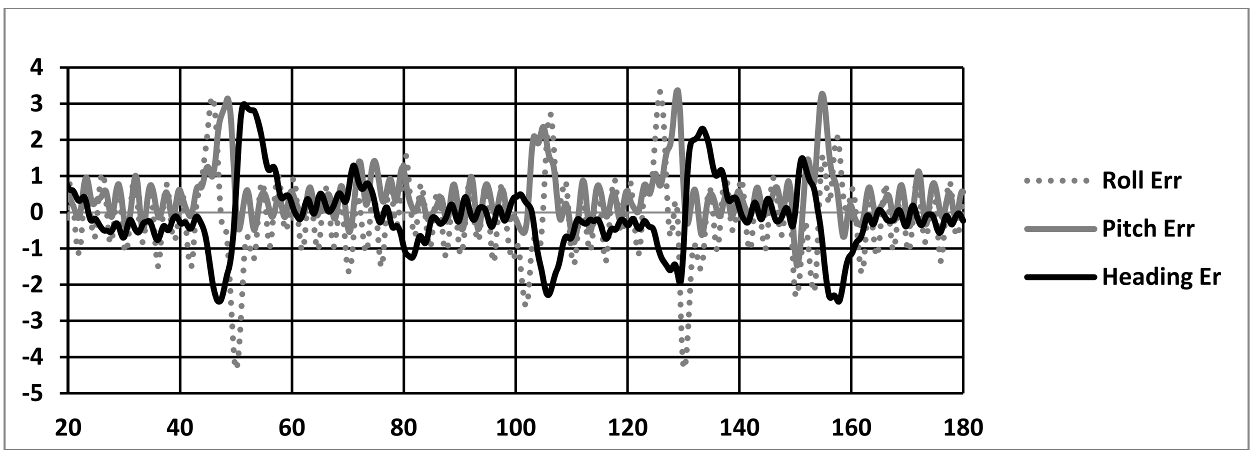

Fig. 10 - Roll, Pitch, Heading Error (deg) vs. Time (sec)
With 10 Ft And 5 Ft GPS-Receiver-To-IMU X, Y Lever Arm Compensation Error

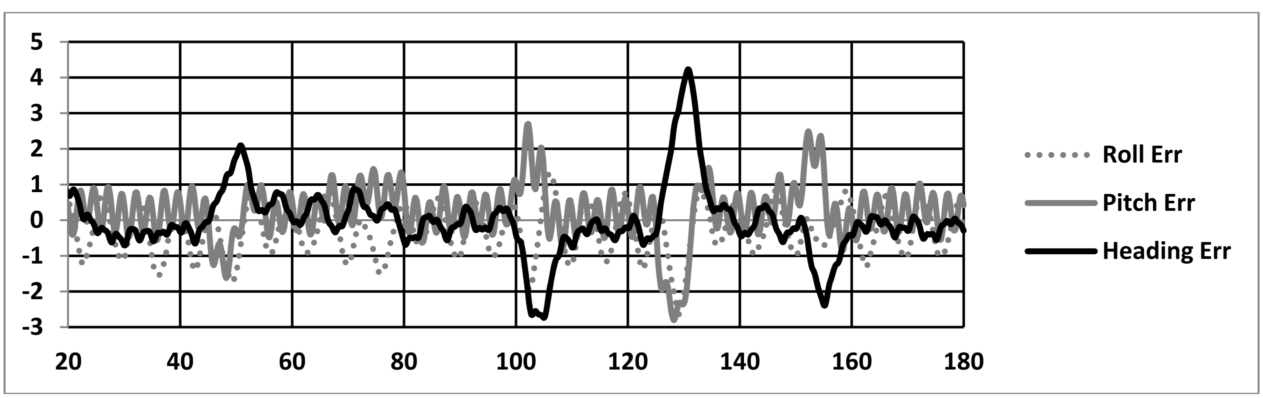

Fig. 11 - Roll, Pitch, Heading Error (deg) vs. Time (sec)
With 5 Deg IMU-To-Magnetometer Heading Misalignment

11.6.2 Error Sources Requiring Continuous Auto Compensation During FGAHRS Usage

For contrast with Fig. 9c, Figs. 12 - 13 have been prepared illustrating the impact on FGAHRS attitude accuracy of leaving gyro/accelerometer bias errors uncalibrated at 10 deg/sec and 10 milli-gs (compared with the calibrated Section 11.4.1 values used in Fig. 9c). For each of Figs. 12 - 13, the resulting attitude errors are somewhat larger than the 1 deg error levels achieved by the performance baseline in Fig. 9c (but still generally acceptable).

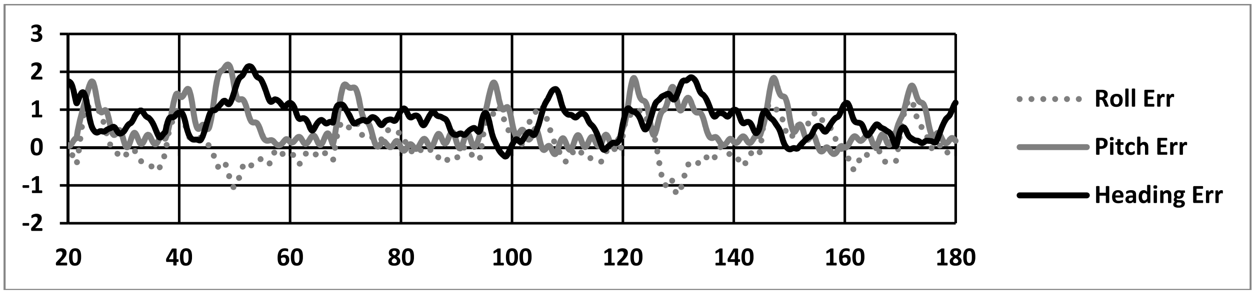

Fig. 12 - Roll, Pitch, Heading Error (deg) vs. Time (sec)
With 1 Deg Per Sec X, Y, Z Gyro Bias Error

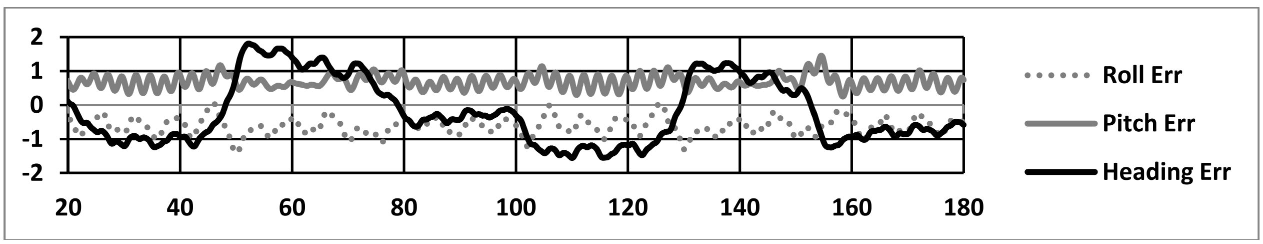

Fig. 13 - Roll, Pitch, Heading Error (deg) vs. Time (sec)
With 10 milli-g Additional X and Y Accelerometer Bias Error

11.6.3 Addition Of Auto Gyro Bias Compensation

Figs. 14a and 14b are a repeat of Fig. 12 operation with 1 deg/sec gyro bias error, but in this case, having the Section 9 FGAHRS auto gyro bias compensation process engaged. Fig. 14a shows the resulting attitude error history and Fig. 14b shows the corresponding auto gyro bias compensation value history. Fig. 14a shows that auto gyro bias compensation reduces the 2 deg error values in Fig. 12 to the 1 deg levels of the Fig. 9c baseline (that were based on 0.1 deg/sec calibrated gyros). Fig. 14b shows how auto gyro bias compensation develops along the trajectory from zero at trajectory start to the 1 deg/sec level needed for accurate compensation of the 1 deg/sec gyro errors.

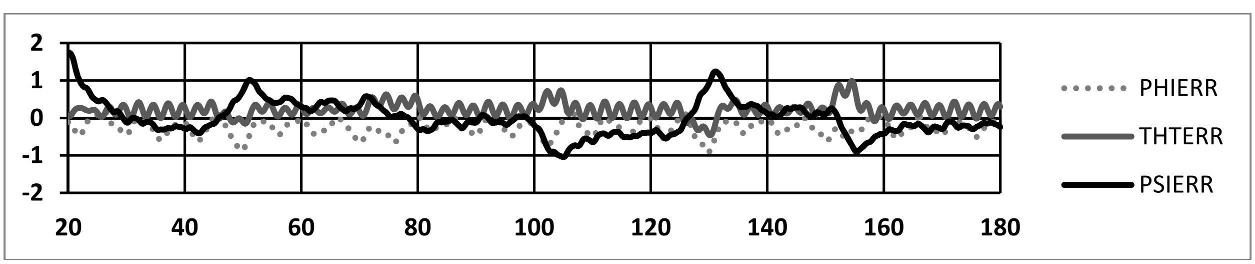

Fig. 14a - Roll, Pitch, Heading Error (deg) vs. Time (sec)
With 1 Degree Per Second X, Y, Z Gyro Bias Error
With Auto Gyro Bias Compensation

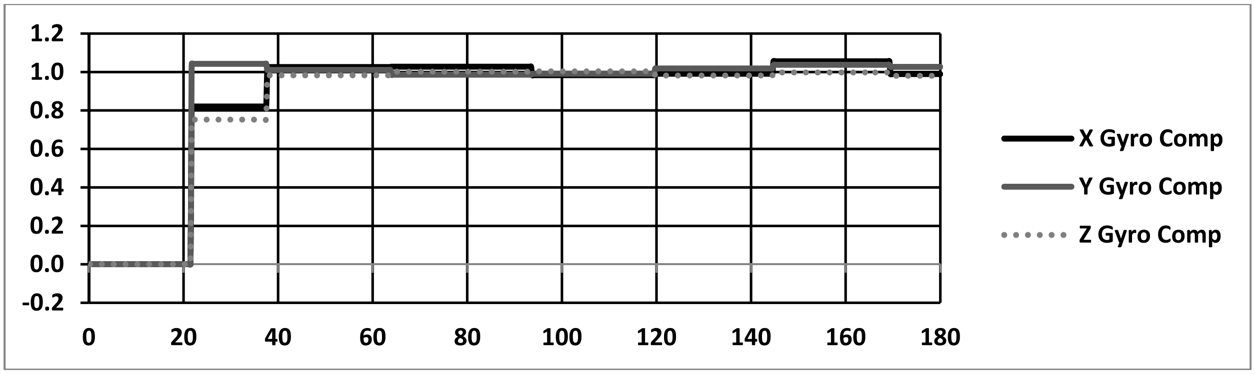

Fig. 14b - Auto Gyro Bias Compensation (deg/sec) vs. Time (sec)
With 1 Degree Per Second X, Y, Z Gyro Bias Error

11.6.4 Addition Of Auto Accelerometer Bias Compensation

A forthcoming article will describe in-use auto compensation for the accelerometers, illustrating how it would compensate the 10 milli-g accelerometer errors used in Fig. 13 to the 3 milli-g level used for Fig. 9c FGAHRS baseline performance evaluation.

11.6.5 The Effect Of Increased Magnetic Field Inclination From Vertical

Thus far, all baseline data presented was for a trajectory located at 30 deg N latitude and 93 deg W longitude. As discussed in Section 10, operation at higher latitudes increases the magnetic field inclination angle from vertical (e.g., from 58.9 deg at 30 deg N latitude to 74.7 deg at 50 deg N latitude). The effect increases the coupling of attitude tilt around the north axis into the magnetometer derived heading error measurement (by the tangent of the inclination angle – see (B-3) of Appendix B). Figs. 9a and 9b show that the effect at 30 deg latitude increases the magnitude of the initial heading error under large roll/pitch angles (through the Section 5.1 FGAHRS coarse attitude alignment initialization process). In other respects, the effect wasn't strong enough under baseline conditions to appreciably impact the ability for sustained 1 deg attitude accuracy in Fig. 9c following initialization transient convergence.

11.6.5.1 Increasing Magnetic Field Inclination For Compensated (Baseline) Accelerometer Bias

Figs. 15a and 15b illustrate how performance would be impacted by operating the FGAHRS baseline at 50 deg N latitude with its corresponding increased magnetic field inclination angle (to 74.71 deg - compared with the 58.94 deg inclination in Figs. 9a - 9c for 30 deg latitude operation). Comparing Fig. 15a with Fig. 9a shows that increased latitude generates a much larger initial heading error (from -12 to -30 deg) which is still effectively converged by the FGAHRS fixed gain control loops. Fig. 15b shows that the converged heading error would then be 1.5 deg compared to 1 deg for 30 N latitude operation illustrated in Fig. 9c, still reasonably acceptable performance.

Increased heading error in Fig. 15b (compared to Fig. 9c) is primarily caused by the 3 milli-g horizontal accelerometer errors present in these runs (through north attitude tilt coupling into heading error, then heading error coupling into north and east attitude tilt during trajectory turns). The 3 milli-g values are based on accelerometer biases having been in-use auto compensated from their potentially uncompensated values of 10 milli-gs (for commercially available MEMS accelerometers).

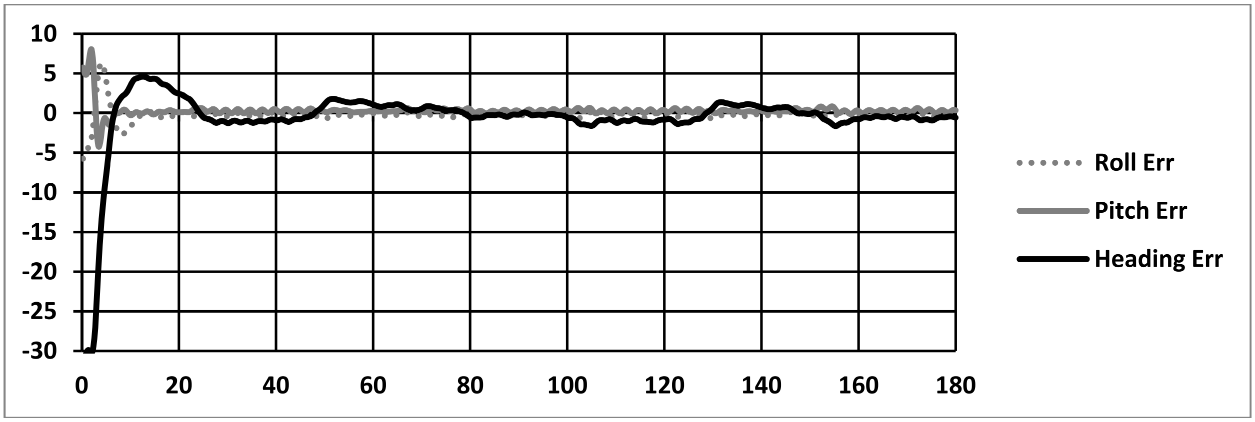

Fig. 15a - Roll, Pitch, Heading Error (deg) vs. Time (sec)
Baseline Error Conditions
At 50 Deg N Latitude / 93 W Longitude
Time Scale = 0 to 180 Seconds

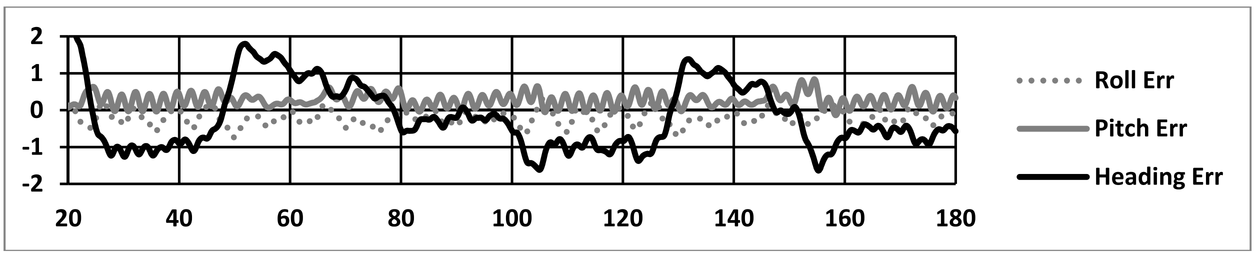

Fig. 15b - Roll, Pitch, Heading Error (deg) vs. Time (sec)
Baseline Error Conditions
At 50 Deg N Latitude / 93 W Longitude
Time Scale = 20 to 180 Seconds

11.6.5.2 Increasing Magnetic Field Inclination For Un-Compensated Accelerometer Bias

Fig. 16 shows that for 10 milli-g accelerometer bias at 50 Deg N Latitude / 93 W Longitude (and a corresponding 74.7 deg magnetic field inclination angle), FGAHRS heading error would be 4 deg without auto accelerometer bias compensation, significantly larger than the 1.5 deg heading error shown in Fig. 15b with compensated accelerometer bias. The result illustrates that for accelerometers having commercial grade MEMS accelerometers of unstable 10 milli-g (or larger) bias error, in-use auto bias calibration is required to sustain accurate heading during operation at high north (and south) latitudes. A subsequent article will show how in-use auto accelerometer bias compensation (based on least squares error estimation) can be incorporated into the FGAHRS computational software.

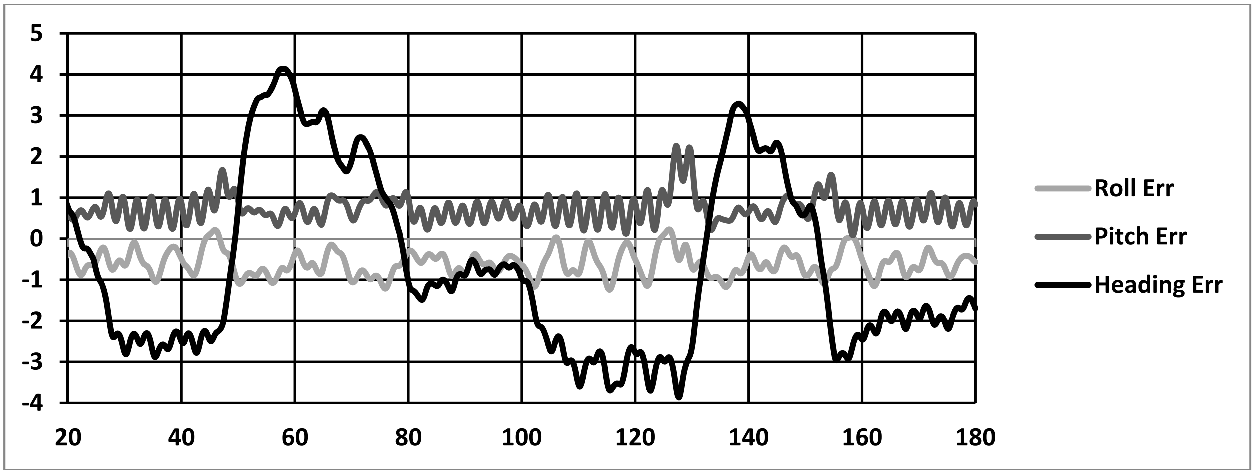

Fig. 16 - Roll, Pitch, Heading Error (deg) vs. Time (sec)
With 10 milli-g Additional X and Y Accelerometer Bias Error
At 50 Deg N Latitude / 93 W Longitude
Time Scale = 20 to 180 Seconds

11.6.6 <u>The Effect Of Increased Trajectory Oscillation Amplitudes</u>

Te trajectory used for each of the previously presented performance evaluations contained 3-axis linear and angular oscillations with peak-to-peak amplitudes as defined in Section 11.1 (20 deg for pitch and roll, 6 deg for heading, 1 ft for X, Y axis and 2 ft for Z axis linear oscillations. This sections shows how baseline FGAHRS performance in Figs. 9a – 9c is impacted by doubling these oscillation amplitudes. Results are presented in Figs. 17a – 17c. Compared to the Fig. 9a and 9c results, Figs. 17a – 17c show comparable 1 deg accuracy following initial transient decay, but with a larger initial transient amplitude due to the Section 5.1 coarse attitude initialization process in the presence of the larger angular oscillations.

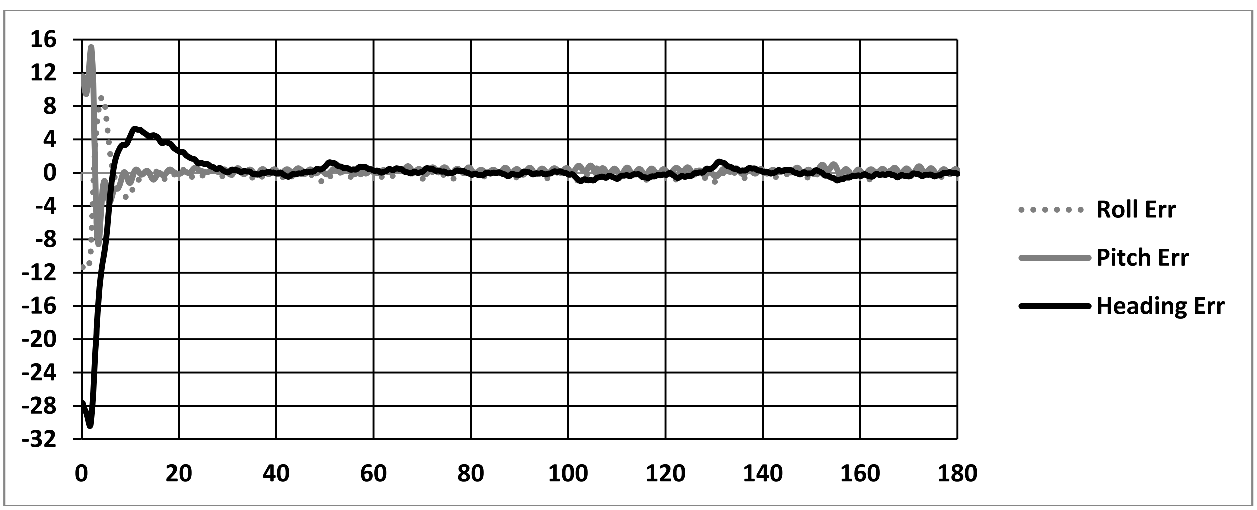

Fig. 17a - Roll, Pitch, Heading Error (deg) vs. Time (sec)
With Doubling Of Oscillation Amplitudes
Time Scale = 0 to 180 Seconds

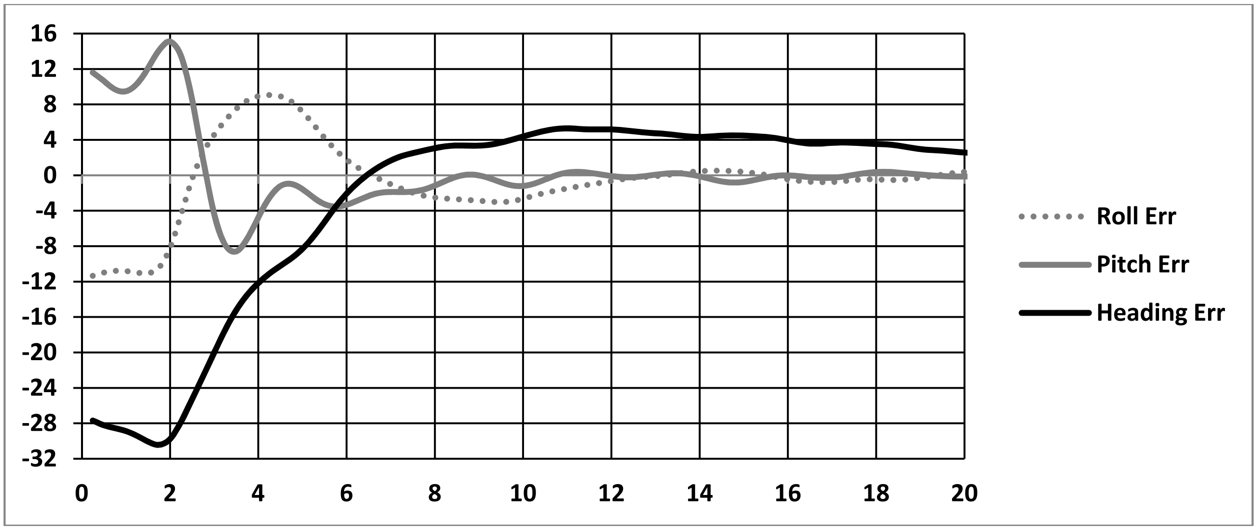

Fig. 17b - Roll, Pitch, Heading Error (deg) vs. Time (sec)
With Doubling Of Oscillation Amplitudes
Time Scale = 0 to 20 Seconds

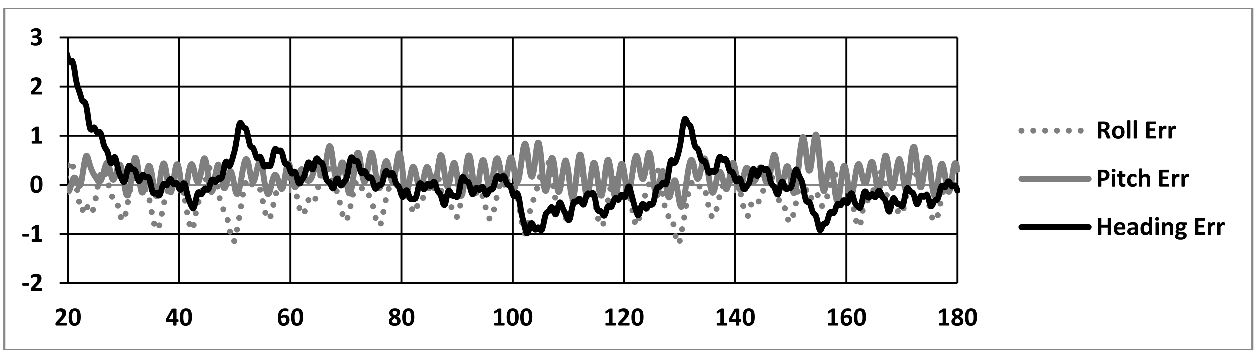

Fig. 17c - Roll, Pitch, Heading Error (deg) vs. Time (sec)
With Doubling Of Oscillation Amplitudes
Time Scale = 20 to 180 Seconds

12. CONCLUSIONS

The fixed gain approach described in this article is a viable and direct method for implementing a strapdown attitude/heading reference system (FGAHRS) for operation in dynamically moving surface vehicles (at sea or on land) using commercially available strapdown MEMS inertial sensors, a 3-axis strapdown magnetometer (for heading error reference feedback), and GPS horizontal velocity (for attitude tilt error control feedback). FGAHRS roll, pitch, heading accuracy on the order of 1 deg should be readily achievable under dynamic trajectory conditions. Operation at high northern or southern latitudes (e.g., 50 deg) will degrade accuracy to some extent, but to a still acceptable level (e.g., to 1.5 deg heading accuracy).

The 1 to 1.5 deg FGAHRS accuracy figures assume application of auto gyro and accelerometer bias compensation routines within the FGAHRS software for continuous in-use reduction of unstable bias errors (from 1 deg/sec, 10 milli-gs uncompensated values to 0.1 deg/sec, 3 milli-gs with auto compensation). The auto gyro bias compensation routine used to generate the Figs.14a and 14b performance data has been described in Section 9 of this article. A subsequent article will define how auto accelerometer bias compensation can be implemented within the FGAHRS software based on least squares estimation, demonstrating performance improvement achievable under dynamic trajectory conditions.

Another future article will provide a detailed analytical definition of the trajectory generator used in this article to create simulated FGAHRS strapdown IMU inertial sensor, 3-axis strapdown magnetometer, and GPS horizontal velocity inputs, with a corresponding "truth model" attitude, velocity, position history for FGAHRS performance comparison.

APPENDIX A

FGAHRS OPEN-LOOP ERROR EQUATIONS DERIVATION

Derivation of the error equations for open-loop FGAHRS response begins by taking the error differential of $\underline{R}^N_{Resid\,H}$ and the C^N_B, $\underline{v}^N_H$, $\Delta\underline{R}^N_{woLv\,H}$ integrands in Fig. 4, excluding feedbacks:

$$\begin{aligned}
\delta\dot{C}^N_B &= \delta\left[C^N_B\left(\underline{\omega}^B_{Gyro}\times\right)\right] = \delta C^N_B\left(\underline{\omega}^B_{Gyro}\times\right) + C^N_B\left(\delta\underline{\omega}^B_{Gyro}\times\right) \\
\delta\dot{\underline{v}}^N_H &= \delta\left(C^N_B\underline{a}^B_{Accel}\right)_H = \left(\delta C^N_B\underline{a}^B_{Accel}\right)_H + \left(C^N_B\delta\underline{a}^B_{Accel}\right)_H \\
\delta\Delta\dot{\underline{R}}^N_{woLv\,H} &= \delta\underline{v}^N_H - \delta\underline{v}^N_{GPS\,H} \\
\delta\underline{R}^N_{Resid\,H} &= \delta\Delta\underline{R}^N_{woLv\,H} - \left(C^N_B\,\delta\underline{l}^B\right)_H + \left(C^N_B\,\delta\underline{l}^B\right)_{H0}
\end{aligned} \qquad \text{(A-1)}$$

where δ identifies the error in the associated parameter. The δC^N_B error in C^N_B is traditionally represented in terms of small angle error vector $\underline{\gamma}^N$ defined as an angular rotation of the N frame such that $\hat{C}^N_B$, the matrix including error, equals $\left[I - \left(\underline{\gamma}^N\times\right)\right]C^N_B$, where $\left[I - \left(\underline{\gamma}^N\times\right)\right]$ is a small angle direction matrix that rotates the correct C^N_B into $\hat{C}^N_B$ - as in [1, Eq. (3.5.2-11)]. Thus, $\delta C^N_B \equiv \hat{C}^N_B - C^N_B$, and

$$\delta C^N_B \equiv -\left(\underline{\gamma}^N\times\right)C^N_B \qquad \text{(A-2)}$$

With (A-2), the $\delta\dot{C}^N_B$ expression in (A-1) becomes

$$\delta\dot{C}^N_B = -\left(\underline{\gamma}^N\times\right)C^N_B\left(\underline{\omega}^B_{Gyro}\times\right) + C^N_B\left(\delta\underline{\omega}^B_{Gyro}\times\right) \qquad \text{(A-3)}$$

Using [1, Eq. (3.3.2-9)] for $\dot{C}^N_B$, the derivative of (A-2) finds for $\delta\dot{C}^N_B$:

$$\delta \dot{C}_B^N = -\left(\underline{\dot{\gamma}}^N \times\right) C_B^N - \left(\underline{\gamma}^N \times\right) \dot{C}_B^N = -\left(\underline{\dot{\gamma}}^N \times\right) C_B^N - \left(\underline{\gamma}^N \times\right) C_B^N \left(\underline{\omega}_{Gyro}^B \times\right) \quad \text{(A-4)}$$

Equating (A-3) to (A-4):

$$\delta \dot{C}_B^N = -\left(\underline{\dot{\gamma}}^N \times\right) C_B^N - \left(\underline{\gamma}^N \times\right) \dot{C}_B^N = -\left(\underline{\dot{\gamma}}^N \times\right) C_B^N - \left(\underline{\gamma}^N \times\right) C_B^N \left(\underline{\omega}_{Gyro}^B \times\right) \quad \text{(A-5)}$$

After canceling like terms, the negative of (A-5) becomes:

$$\left(\underline{\dot{\gamma}}^N \times\right) C_B^N = -\, C_B^N \left(\delta \underline{\omega}_{Gyro}^B \times\right) \quad \text{(A-6)}$$

Multiplying (A-6) on the right by the transpose of C_B^N (equal to its negative for a direction cosine matrix) while recognizing from [1, Eq. (3.1.1-38)] that similarity transformation $C_B^N \left(\delta \underline{\omega}_{Gyro}^B \times\right) \left(C_B^N\right)^T$ equates to $\left[\left(C_B^N \delta \underline{\omega}_{Gyro}^B\right) \times\right]$, then obtains

$$\left(\underline{\dot{\gamma}}^N \times\right) = -\left[\left(C_B^N \, \delta \underline{\omega}_{Gyro}^B\right) \times\right] \quad \text{(A-7)}$$

or finally,

$$\underline{\dot{\gamma}}^N = -\, C_B^N \, \delta \underline{\omega}_{Gyro}^B \quad \text{(A-8)}$$

The horizontal (*H*) and downward (*Down*) components of A-8) are

$$\underline{\dot{\gamma}}_H^N = -\left(C_B^N \, \delta \underline{\omega}_{Gyro}^B\right)_H \qquad \gamma_{Down}^N = \int_0^t \dot{\gamma}_{Down}^N \, dt \quad \text{(A-9)}$$

With (A-2), the $\delta \underline{\dot{v}}_H^N$ expression in (A-1) becomes

$$\begin{aligned} \delta \underline{\dot{v}}_H^N &= \left(\delta C_B^N \, \underline{a}_{Accel}^B\right)_H + \left(C_B^N \delta \underline{a}_{Accel}^B\right)_H = -\left[\left(\underline{\gamma}^N \times\right) C_B^N \underline{a}_{Accel}^B\right]_H + \left(C_B^N \delta \underline{a}_{Accel}^B\right)_H \\ &= -\left(\underline{\gamma}^N \times \underline{a}_{Accel}^N\right)_H + \left(C_B^N \delta \underline{a}_{Accel}^B\right)_H \end{aligned} \quad \text{(A-10)}$$

Define $\underline{\gamma}^N$ and $\underline{a}_{Accel}^N$ as the sum of their horizontal and downward vertical components:

$$\underline{\gamma}^N = \underline{\gamma}_H^N + \gamma_{Down}^N \, \underline{u}_{Down}^N \qquad \underline{a}_{Accel}^N = \underline{a}_{Accel\,H}^N + a_{Accel\,Down}^N \, \underline{u}_{Down}^N \quad \text{(A-11)}$$

where $\underline{u}^N_{Down}$ is a unit vector downward (along the N frame z axis). With (A-11), (A-10) becomes

$$\begin{aligned} \delta\dot{\underline{v}}^N_H &= -\left[\left(\underline{\gamma}^N_H + \gamma^N_{Down}\,\underline{u}^N_{Down}\right)\times\left(\underline{a}^N_{Accel\,H} + a^N_{Accel\,Down}\,\underline{u}^N_{Down}\right)\right]_H + \left(C^N_B\delta\underline{a}^B_{Accel}\right)_H \\ &= -\,a^N_{Accel\,Down}\,\underline{\gamma}^N_H\times\underline{u}^N_{Down} - \gamma^N_{Down}\,\underline{u}^N_{Down}\times\underline{a}^N_{Accel\,H} + \left(C^N_B\delta\underline{a}^B_{Accel}\right)_H \end{aligned} \qquad \text{(A-12)}$$

Lastly, we approximate $a^N_{Accel\,Down}$ as 1 g upward (to balance downward gravity) so that (A-12) simplifies to

$$\delta\dot{\underline{v}}^N_H \approx g\;\underline{\gamma}^N_H\times\underline{u}^N_{Down} - \gamma^N_{Down}\,\underline{u}^N_{Down}\times\underline{a}^N_{Accel\,H} + \left(C^N_B\,\delta\underline{a}^B_{Accel}\right)_H \qquad \text{(A-13)}$$

In summary, the results in (A-9) and (A-13) with (A-1) for $\delta\underline{R}^N_{Resid\,H}$ and $\delta\Delta\dot{\underline{R}}^N_{woLv\,H}$ (including subscript 0 initialization errors), are:

$$\begin{gathered} \dot{\underline{\gamma}}^N_H = -\left(C^N_B\,\delta\underline{\omega}^B_{Gyro}\right)_H \qquad \gamma^N_H = \gamma^N_{H\,0} + \int_0^t \dot{\underline{\gamma}}^N_H\,dt \\ \dot{\gamma}^N_{Down} = -\left(C^N_B\,\delta\underline{\omega}^B_{Gyro}\right)_{Down} \qquad \gamma^N_{Down} = \gamma^N_{Down0} + \int_0^t \dot{\gamma}^N_{Down}\,dt \\ \delta\dot{\underline{v}}^N_H \approx \left(C^N_B\,\delta\underline{a}^B_{Accel}\right)_H + g\;\underline{\gamma}^N_H\times\underline{u}^N_{Down} - \gamma^N_{Down}\,\underline{u}^N_{Down}\times\underline{a}^N_{Accel\,H} \\ \delta\underline{v}^N_H = \delta\underline{v}^N_{H\,0} + \int_0^t \delta\dot{\underline{v}}^N_H dt \\ \delta\dot{\underline{R}}^N_{woLv\,H} = \delta\underline{v}^N_H - \delta\underline{v}^N_{GPS\,H} \qquad \delta\underline{R}^N_{woLv\,H} = \delta\underline{R}^N_{woLv/H\,0} + \int_0^t \delta\dot{\underline{R}}^N_{woLv\,H}\,dt \\ \delta\underline{R}^N_{Resid\,H} = \delta\Delta\underline{R}^N_{woLv\,H} - \left(C^N_B\,\delta\underline{l}^B\right)_H + \left(C^N_B\,\delta\underline{l}^B\right)_{H\,0} \end{gathered} \qquad \text{(A-14)}$$

APPENDIX B

CLOSED-LOOP FGAHRS ERROR EQUATIONS DERIVATION

Derivation of the error equations for closed-loop FGAHRS response begins with the error differential of the C^N_B, $\underline{v}^N_H$, $\Delta\underline{R}^N_{woLv\,H}$ integrands in Fig. 4, blocks 1 and 3, including the differential of $\underline{R}^N_{Resid\,H}$ in block 3, and using $\delta\psi_{resid}$ from (C-10) Appendix C for the differential of ψ_{resid} in block 3:

$$\delta \dot{C}_B^N = \delta\left[C_B^N \left(\underline{\omega}_{Gyro}^B \times \right) - \left(\underline{\omega}_{FB}^N \times \right) C_B^N \right]$$
$$= \delta C_B^N \left(\underline{\omega}_{Gyro}^B \times \right) + C_B^N \left(\delta \underline{\omega}_{Gyro}^B \times \right) - \left(\delta \underline{\omega}_{FB}^N \times \right) C_B^N - \left(\underline{\omega}_{FB}^N \times \right) \delta C_B^N \qquad \text{(B-1)}$$

$$\delta \dot{\underline{v}}_H^N = \delta\left(C_B^N \underline{a}_{Accel}^B - \dot{\underline{v}}_{H_{FB}}^N \right)_H = \left(\delta C_B^N \underline{a}_{Accel}^B \right)_H + \left(C_B^N \delta \underline{a}_{Accel}^B \right)_H - \delta \dot{\underline{v}}_{H_{FB}}^N \qquad \text{(B-2)}$$

$$\delta \dot{\underline{R}}_{woLv_H}^N = \delta \underline{v}_H^N - \delta \underline{v}_{GPS_H}^N - \Delta \dot{\underline{R}}_{woLv/H_{FB}}^N$$
$$\delta \underline{R}_{Resid_H}^N = \delta \underline{R}_{woLv_H}^N - \delta\left(C_B^N \underline{l}^B \right)_H + \delta\left(C_B^N \underline{l}^B \right)_{H_0} \qquad \text{(B-3)}$$
$$\delta \dot{\underline{v}}_{H_{FB}}^N = K_v \, \delta \underline{R}_{Resid_H}^N \qquad \delta \Delta \dot{\underline{R}}_{woLv/H_{FB}}^N = K_R \, \delta \underline{R}_{Resid_H}^N$$

$$\delta \underline{\omega}_{FB}^N = -K_{\gamma_H} \, \underline{u}_{Down}^N \times \delta \underline{R}_{Resid_H}^N + K_{\gamma_\psi} \, \delta\psi_{Resid} \, \underline{u}_{Down}^N + \delta \underline{\omega}_{BiasFB}^N$$
$$\delta \dot{\underline{\omega}}_{BiasFB}^N = -K_{\omega Bias_H} \, \underline{u}_{Down}^N \times \delta \underline{R}_{Resid_H}^N + K_{\omega Bias_\psi} \, \delta\psi_{Resid} \, \underline{u}_{Down}^N \qquad \text{(B-4)}$$
$$\delta\psi_{resid} = -\gamma_{dwn}^N + \tan\theta_{incln} \, \gamma_{nrth}^N + \frac{\underline{u}_{east}^N \cdot \left(C_B^N \, \delta \underline{u}_{mag}^B \right)}{u_{mag_{nrth}}^N}$$

Using (A-2), (A-4), and the $\dot{\underline{\gamma}}^N$ derivation procedure in Appendix A, the (B-1) $\delta \dot{C}_B^N$ equation becomes

$$-\left(\dot{\underline{\gamma}}^N \times \right) C_B^N - \left(\underline{\gamma}^N \times \right) C_B^N \left(\underline{\omega}_{Gyro}^B \times \right)$$
$$= -\left(\underline{\gamma}^N \times \right) C_B^N \left(\underline{\omega}_{Gyro}^B \times \right) + C_B^N \left(\delta \underline{\omega}_{Gyro}^B \times \right) - \left(\delta \underline{\omega}_{FB}^N \times \right) C_B^N \qquad \text{(B-5)}$$

After like-term cancellation and multiplication on the right by $\left(C_B^N \right)^T$:

$$-\left(\dot{\underline{\gamma}}^N \times \right) = \left[\left(C_B^N \, \delta \underline{\omega}_{Gyro}^B \right) \times \right] - \left(\delta \underline{\omega}_{FB}^N \times \right) \qquad \text{(B-6)}$$

from which $\dot{\underline{\gamma}}^N$ is obtained:

$$\dot{\underline{\gamma}}^N = -C_B^N \, \delta \underline{\omega}_{Gyro}^B + \delta \underline{\omega}_{FB}^N \qquad \text{(B7)}$$

Substituting $\delta \underline{\omega}_{BiasFB}^N$, $\delta \dot{\underline{\omega}}_{BiasFB}^N$, and $\delta\psi_{resid}$ from (B-4) with $\delta \underline{R}_{Resid_H}^N$ from (B-3) into (B-7) finds for $\dot{\underline{\gamma}}^N$ (and for $\delta \dot{\underline{\omega}}_{BiasFB}^N$):

$$\delta\underline{\dot{\omega}}^{N}_{BiasFB} = -K_{\omega Bias_H}\,\underline{u}^{N}_{Down}\times\left[\delta\underline{R}^{N}_{woLv_H} - \delta\left(C^{N}_{B}\underline{l}^{B}\right)_{H} + \delta\right]\left(C^{N}_{B}\underline{l}^{B}\right)_{H_0}$$

$$- K_{\omega Bias_\psi}\left(\gamma^{N}_{dwn} - \tan\theta_{incln}\,\gamma^{N}_{nrth} - \frac{\underline{u}^{N}_{east}\cdot\left(C^{N}_{B}\,\delta\underline{u}^{B}_{mag}\right)}{u^{N}_{mag_{nrth}}}\right)\underline{u}^{N}_{Down}$$

$$\underline{\dot{\gamma}}^{N} = -C^{N}_{B}\,\delta\underline{\omega}^{B}_{Gyro} - K_{\gamma_H}\,\underline{u}^{N}_{Down}\times\left[\delta\underline{R}^{N}_{woLv_H} - \delta\left(C^{N}_{B}\underline{l}^{B}\right)_{H} + \delta\right]\left(C^{N}_{B}\underline{l}^{B}\right)_{H_0} \tag{B-8}$$

$$- K_{\gamma_\psi}\left(\gamma^{N}_{dwn} - \tan\theta_{incln}\,\gamma^{N}_{nrth} - \frac{\underline{u}^{N}_{east}\cdot\left(C^{N}_{B}\,\delta\underline{u}^{B}_{mag}\right)}{u^{N}_{mag_{nrth}}}\right)\underline{u}^{N}_{Down} + \delta\underline{\omega}^{N}_{BiasFB}$$

The $\delta C^{N}_{B}\,\underline{a}^{B}_{Accel}$ term in $\delta\underline{\dot{v}}^{N}_{H}$ of (B-2) is the same as in (A-13) with which (B-2) becomes:

$$\delta\underline{\dot{v}}^{N}_{H} \approx g\,\underline{\gamma}^{N}_{H}\times\underline{u}^{N}_{Down} - \gamma^{N}_{Down}\,\underline{u}^{N}_{Down}\times\underline{a}^{N}_{Accel_H} + \left(C^{N}_{B}\,\delta\underline{a}^{B}_{Accel}\right)_{H} - \delta\underline{\dot{v}}^{N}_{H_{FB}} \tag{B-9}$$

Substituting $\delta\underline{\dot{v}}^{N}_{H_{FB}}$ from (B-4) with $\delta\underline{R}^{N}_{Resid_H}$ from (B-3) into (B-9) finds for $\delta\underline{\dot{v}}^{N}_{H}$:

$$\delta\underline{\dot{v}}^{N}_{H} = \left(\delta C^{N}_{B}\,\underline{a}^{B}_{Accel}\right)_{H} + \left(C^{N}_{B}\,\delta\underline{a}^{B}_{Accel}\right)_{H} - K_{v}\left[\delta\underline{R}^{N}_{woLv_H} - \delta\left(C^{N}_{B}\underline{l}^{B}\right)_{H} + \delta\left(C^{N}_{B}\,\underline{l}^{B}\right)_{H_0}\right] \tag{B-10}$$

Substituting $\delta\underline{\dot{R}}^{N}_{woLv_H}$ from (B-4) with $\delta\underline{R}^{N}_{Resid_H}$ from (B-3) into (B-3) finds for $\delta\underline{\dot{R}}^{N}_{woLv_H}$:

$$\delta\underline{\dot{R}}^{N}_{woLv_H} = \delta\underline{v}^{N}_{H} - \delta\underline{v}^{N}_{GPS_H} - K_{R}\left[\delta\underline{R}^{N}_{woLv_H} - \delta\left(C^{N}_{B}\,\underline{l}^{B}\right)_{H} + \delta\left(C^{N}_{B}\,\underline{l}^{B}\right)_{H_0}\right] \tag{B-11}$$

The horizontal (H) and vertical (down) components of (B-9) – (B-11) then summarize as follows:

$$\delta\underline{\dot{\omega}}_{BiasFB_H}^{N} = -K_{\omega Bias_H}\,\underline{u}_{Down}^{N} \times \delta\Delta\underline{R}_{woLv_H}^{N}$$

$$+ K_{\omega Bias_H}\,\underline{u}_{Down}^{N} \times \left[\left(C_B^N \delta\underline{l}^B\right)_H - \left(C_B^N \delta\underline{l}^B\right)_{H0}\right]$$

$$\underline{\dot{\gamma}}_H^N = -\left(C_B^N\,\delta\underline{\omega}_{Gyro}^B\right)_H + \delta\underline{\omega}_{BiasFB_H}^N - K_{\gamma_H}\,\underline{u}_{Down}^N \times \delta\Delta\underline{R}_{woLv_H}^N$$

$$+ K_{\gamma_H}\,\underline{u}_{Down}^N \times \left[\left(C_B^N \delta\underline{l}^B\right)_H - \left(C_B^N \delta\underline{l}^B\right)_{H0}\right]$$

$$\delta\underline{\dot{v}}_H^N \approx \left(C_B^N \delta\underline{a}_{Accel}^B\right)_H - K_v\,\delta\Delta\underline{R}_{woLv_H}^N + g\,\underline{\gamma}_H^N \times \underline{u}_{Down}^N - \gamma_{Down}^N\,\underline{u}_{Down}^N \times \underline{a}_{Accel\,H}^N$$

$$+ K_v\left[\left(C_B^N\,\delta\underline{l}^B\right)_H - \left(C_B^N\,\delta\underline{l}^B\right)_{H0}\right] \qquad \text{(B-12)}$$

$$\delta\Delta\underline{\dot{R}}_{woLv_H}^N = \delta\underline{v}_H^N - K_R\,\delta\Delta\underline{R}_{woLv_H}^N - \delta\underline{v}_{GPS_H}^N + K_R\left[\left(C_B^N \delta\underline{l}^B\right)_H - \left(C_B^N \delta\underline{l}^B\right)_{H0}\right]$$

$$\delta\dot{\omega}_{BiasFB_{Down}}^N = -K_{\omega Bias_\psi}\left[\gamma_{dwn}^N - \tan\theta_{incln}\,\gamma_{nrth}^N - K_{\omega Bias_\psi}\frac{\underline{u}_{east}^N \cdot \left(C_B^N\,\delta\underline{u}_{mag}^B\right)}{u_{mag_{nrth}}^N}\right]$$

$$\dot{\gamma}_{Down}^N = -\underline{u}_{Down}^N \cdot \left(C_B^N\,\delta\underline{\omega}_{Gyro}^B\right)$$

$$-K_{\gamma_\psi}\left[\gamma_{dwn}^N - \tan\theta_{incln}\,\gamma_{nrth}^N - K_{\gamma_\psi}\frac{\underline{u}_{east}^N \cdot \left(C_B^N\,\delta\underline{u}_{mag}^B\right)}{u_{mag_{nrth}}^N}\right] + \delta\omega_{BiasFB_{Down}}^N$$

APPENDIX C

STRAPDOWN MAGNETOMETER ANALYTICAL MODELING

A strapdown magnetic field detector (magnetometer) consists of three orthogonal sensing elements, each measuring the component of earth's magnetic field along its sensing axis. Earth's magnetic field can be represented in the *N* frame (x north, y east, z down) as a unit vector along the magnetic field direction:

$$\underline{u}_{mag}^N = C_{incln}\,C_{dcln}\,\underline{u}_{nrth}^N \qquad \underline{u}_{nrth}^N = \begin{bmatrix} 1 \\ 0 \\ 0 \end{bmatrix}$$

$$C_{dcln} = \begin{bmatrix} \cos\theta_{dcln} & \sin\theta_{dcln} & 0 \\ -\sin\theta_{dcln} & \cos\theta_{dcln} & 0 \\ 0 & 0 & 1 \end{bmatrix} \quad C_{incln} = \begin{bmatrix} \cos\theta_{incln} & 0 & -\sin\theta_{incln} \\ 0 & 1 & \\ \sin\theta_{incln} & 0 & \cos\theta_{incln} \end{bmatrix} \qquad \text{(C-1)}$$

where $\underline{u}_{mag}^{N}$ is a unit vector along the magnetic field direction in the *N* frame, $\underline{u}_{nrth}^{N}$ is a unit vector along the *N* frame x (north) axis, C_{dcln} is a direction cosine matrix that transforms vectors <u>negatively</u> around the vertically downward *N* frame z axis through the magnetic field declination angle θ_{dcln} (also known as the magnetic variation), and C_{incln} is a direction cosine matrix that transforms vectors <u>negatively</u> around the C_{incln} rotated y (east) axis through magnetic field inclination angle θ_{incln}.

For a magnetic detector used for heading determination, the ideal orientation of the magnetic field is north so that heading variations from north will be detectable as a rotation of the detector from that direction. In addition to a north component, the actual magnetic field has both vertical and east components, the latter being analytically removable based on a priori knowledge of the magnetic field direction (a known numerical function of local latitude and longitude). Combining the terms in (C-1) obtains:

$$\underline{u}_{mag}^{N} = \begin{bmatrix} \cos\theta_{dcln}\cos\theta_{incln} \\ -\sin\theta_{dcln} \\ \cos\theta_{dcln}\sin\theta_{incln} \end{bmatrix} \qquad \text{(C-2)}$$

For the strapdown FGAHRS application, the strapdown magnetic detector triad used for heading determination has its sensing axes aligned with FGAHRS IMU *B* frame axes, thus measuring earth's magnetic field unit vector in *B* frame coordinates ($\underline{u}_{mag}^{B}$). To determine the heading error in computed FGAHRS algorithm attitude, the sensed magnetometer output is transformed to the *N* frame using the FGAHRS computed C_B^N matrix:

$$\underline{u}_{mag}^{N} = C_B^N \, \underline{u}_{mag}^{B} \qquad \text{(C-3)}$$

A $\sin\theta_{dcln}$ correction is applied to the east (y) component of $\underline{u}_{mag}^{N}$ in (C-2), yielding α_{resid}, a result (residual) that would be zero if $\underline{u}_{mag}^{B}$ and C_B^N were error free:

$$\alpha_{resid} = \underline{u}_{east}^{N} \cdot \underline{u}_{mag}^{N} + \sin\theta_{dcln} = \underline{u}_{east}^{N} \cdot \left(C_B^N \, \underline{u}_{mag}^{B} \right) + \sin\theta_{dcln} \qquad \text{(C-4)}$$

Under C_B^N and $\underline{u}_{mag}^{B}$ error conditions, α_{resid} will measure the heading-like error in C_B^N as revealed by the error form (differential) of (C-4). Neglecting the error in $\sin\theta_{dcln}$ finds

$$\delta\alpha_{resid} = \underline{u}_{east}^{N} \cdot \left(\delta C_B^N \, \underline{u}_{mag}^{B} \right) + \underline{u}_{east}^{N} \cdot \left(C_B^N \, \delta\underline{u}_{mag}^{B} \right) \qquad \text{(C-5)}$$

With the inverse (transpose) of (C-3) for $\underline{u}_{mag}^{B}$ and (A-2) for δC_B^N, (C-5) becomes

$$\delta\alpha_{resid} = -\,\underline{u}_{east}^{N} \cdot \left(\underline{\gamma}^{N} \times \underline{u}_{mag}^{N} \right) + \underline{u}_{east}^{N} \cdot \left(C_B^N \, \delta\underline{u}_{mag}^{B} \right) \qquad \text{(C-6)}$$

Expanding vectors $\underline{\gamma}^N$ and $\underline{u}^N_{mag}$ into their N frame components finds

$$\underline{\gamma}^N = \gamma^N_{nrth}\,\underline{u}^N_{nrth} + \gamma^N_{east}\,\underline{u}^N_{east} + \gamma^N_{dwn}\,\underline{u}^N_{dwn}$$
$$\underline{u}^N_{mag} = u^N_{mag_{nrth}}\,\underline{u}^N_{nrth} + u^N_{mag_{east}}\,\underline{u}^N_{east} + u^N_{mag_{dwn}}\,\underline{u}^N_{dwn} \qquad \text{(C-7)}$$

Substituting (C-7) in (C-6) obtains:

$$\delta\alpha_{resid} = -\,u^N_{mag_{nrth}}\,\gamma^N_{dwn} + u^N_{mag_{dwn}}\,\gamma^N_{nrth} + \underline{u}^N_{east}\cdot\left(C^N_B\;\delta\underline{u}^B_{mag}\right) \qquad \text{(C-8)}$$

Now define:

$$\delta\psi_{resid} \equiv \delta\alpha_{resid} \,/\, u^N_{mag_{nrth}} \qquad \text{(C-9)}$$

Using (C-2) for $u^N_{mag_{nrth}}$, (C-8) becomes the final form:

$$\delta\psi_{resid} = -\,\gamma^N_{dwn} + \tan\theta_{incln}\,\gamma^N_{nrth} + \frac{\underline{u}^N_{east}\cdot\left(C^N_B\;\delta\underline{u}^B_{mag}\right)}{u^N_{mag_{nrth}}} \qquad \text{(C-10)}$$

Based on the (C-9) differential error $\delta\psi_{resid}$, the corresponding non-differential ψ_{resid} would be $\psi_{resid} \equiv \alpha_{resid} \,/\, u^N_{mag_{nrth}}$. Then, using (C-4) for α_{resid}, it follows that:

$$\psi_{resid} = \frac{\underline{u}^N_{east}\cdot\left(C^N_B\;\underline{u}^B_{mag}\right) + \sin\theta_{dcln}}{u^N_{mag_{nrth}}} \qquad \text{(C-11)}$$

Eq. (C-11) constitutes the FGAHRS magnetometer measurement equation, yielding zero under nominal (error free conditions). Under off-nominal conditions (i.e., with errors present), (C-11) becomes $\delta\psi_{resid}$ in (C-10), with $\psi_{resid} = \delta\psi_{resid}$ then becoming proportional to the negative of C^N_B vertical (heading) attitude error γ^N_{dwn}, the primary signal being fed back by the FGAHRS heading control loop (plus a cross-coupling term proportional to the C^N_B north angular error γ^N_{nrth}, plus an error induced by $\delta\underline{u}^B_{mag}$, the magnetometer triad's error in measuring $\underline{u}^B_{mag}$). The θ_{dcln} value for (C-11) would be programmed into the FGAHRS computer as a function of local input latitude/longitude supplied by the FGAHRS GPS receiver.

REFERENCES

[1] Savage, P.G., *Strapdown Analytics, Second Edition*, Strapdown Associates, Inc., 2007

[2] Savage, P.G., "Computational Elements For Strapdown Systems", SAI-WBN-14010, May 31, 2015, available for free access at www.strapdownassociates.com.